Master's Degree Thesis in

Measurement Science and Instrumentation

To Measure the Efficiency of Energy Transfer Systems Under External Influences and Model How the Resonance Frequency is Influenced Under Such Conditions

Pramanand Joshi

Department of Physics and Technology

University of Bergen

June 2014

Abstract

Transfer of power wirelessly through magnetic resonance is a hot topic these days not only for low power consumer electronics like laptops, cell phones etc. but also for high power applications like electric cars, trains and for medical implants as well. In the University of Bergen, the magnetic resonance technique has been used for level measurements and may be used for material properties.

Our objective here is the efficient power transfer using printed circuit board (PCB) coils. The study is performed for the efficiency variation with distance in air. The efficiency is found to be maximum at resonance frequency. The effect of the external factors like steel sheet and salt-water solution of fixed concentration is studied. Both of these obstruct the power transfer efficiency to a certain extent. Steel is more obstructive than salt-water solution of the concentration that we have used.

Acknowledgements

First of all, my sincere gratitude goes to supervisor Professor Lars Egil Helseth for suggesting the problem, motivation, inspiration, and valuable feedback during my work. I am grateful to him for strongly recommending for the summer job in Christian Michelsen Research, CMR. It was beneficial in regards to both academically and financially. Secondly, I want to thank Professor Bjørn Tore Hjertaker for providing the space for lab work in the Multiphase laboratory. I am thankful to Associate Professor emeritus Øystein Olsen for helpful discussions regarding Fourier Transform and Signal Processing.

Several other persons have contributed to my work. I also want to thank Werner Olsen for input and ideas on electronics and for helping in designing PCB coil and the department's workshop for constructing Faraday cage. Thank also goes to my friend Parthivendra Upadhyaya for motivation and other supports.

My family members deserve great thanks, especially my wife for her patience, support and understanding even she could not come to Norway.

Lastly, my thanks go to the University of Bergen for providing me the opportunity to study Master’s degree.

Bergen, June 2, 2014, Pramanand Joshi

Contents

List of Figures

List of tables and charts

List of Symbols

Note: The symbols in bold type represent vectors.

Symbol	Quantity	Unit
x,y,z	Cartesian coordinates	m
ϕ	Azimuthal angle	rad
r	Radial coordinate	m
$\boldsymbol{e}_n$	Unit vector in n-direct	
I	Complex unit	
$\boldsymbol{E}$	Electric field	V/m
$\boldsymbol{B}$	Magnetic field	T
$\boldsymbol{P}$	Polarization vector	C/m^2
$\boldsymbol{D}$	Displacement vector	C/m^2
$\boldsymbol{M}$	Magnetization vector	A/m
$\boldsymbol{H}$	H-field	A/m
V	Electric potential, voltage	V
$\boldsymbol{A}$	Magnetic vector potential	Vs/m
ε	Permittivity	C^2/Nm^2
ε_0	Permittivity of free space	C^2/Nm^2
ε_r	Relative permittivity	
μ	Permeability	N/A^2
μ_0	Permeability of free space	N/A^2

μ_r	Relative permeability	
q	Electric charge	C
ρ	Charge density	C/m^3
σ	Conductivity	S/m
$\boldsymbol{F}$	Force	N
$\boldsymbol{J}$	Current density	A/m^2
I	Current	A
u	Energy density	J/m^3
$\boldsymbol{r}$	Position vector	m
$\boldsymbol{v}$	Velocity	m/s
$\boldsymbol{S}$	Area vector	m^2
V	Volume	m^3
d$\boldsymbol{r}$	Infinitesimal displacement	m
d$\boldsymbol{l}$	Infinitesimal line element	m
d$\boldsymbol{s}$ or d$\boldsymbol{a}$	Infinitesimal area element	m^2
$d\tau$	Infinitesimal volume element	m^3
t	Time	s
f	Frequency	Hz
ω	Angular frequency	rad/s
ω_0	Angular resonance frequency	rad/s
T	Period	s
Λ	Wavelength	m
Φ	Phase constant	rad
C	Speed of light	m/s

Δ	Skin depth	m
R	Resistance	Ω
Φ	Magnetic flux	Wb
L	Self inductance	H
M	Mutual inductance	H
C	Capacitance	F
Z	Impedance	Ω
N	Number of windings	
L	Length of coil	m
Q	Quality factor (Q factor)	
C_0	Inter-winding capacitance, constant part	F

List of Acronyms

Acronym	Explanation
PMMA	Poly-Methyl Meth-Acrylate (also called plexiglass)
RLC	Electric circuit with resistive, inductive and capacitive elements
MIT	Massachusetts Institute of Technology
OEM	Original Equipment Manufacturer
WPC	Wireless Power Consortium
EV	Electric Vehicle
UV	Ultra-Violet
PMC	Perfect Magnetic Conductor
CMT	Coupled Mode Theory
USB	Universal Serial Bus

Chapter 1: Introduction

1.1 Background

Wireless power transfer is of growing interest these days among researchers and the companies involved in power related production. Wireless technology is not as new as one might think; Nikola Tesla performed experiments with it in the late Nineteenth century and was able to transfer [21]. It is apparent that wireless power has not been realized at a consumer level and the concept was almost forgotten after Tesla. Induction stoves and transformers transfer power "wirelessly" and have been around for some time but they all work over negligible distances. After more than a century later, in 2007 Physicists of MIT started research on transfer of power wirelessly using magnetic resonance and presented results of so-called mid-range transfer where transfer distances were up to a couple of meters, a few times the size of coils [1]. The basis of their research is coupled mode theory (CMT). Since then interest in this technology has been boomed up because of its applications in areas ranging from low power consumer electronic devices like mobile devices like cell phones, tablets, laptops, sensors and medical implants to high power applications: electric cars, trains and buses. Several researches are being conducted by the researchers and institutions using CMT. However, coupled inductance model in circuit theory has also been used to analyze the power transfer efficiency of this technology, instead of using coupled mode theory (CMT) [*17*].

To extend the distance of power delivery or increase power transfer efficiency, a resonant coil system with the same resonant frequency can be placed in between transmitter and receiver resonant coils. High-Q capacitors are to be added to the coils in order to adjust the resonant frequency of the resonant coils and reduce the worse effects on power transfer. Otherwise, variation in the resonant frequency caused by external objects is increased due to the small amount of self-capacitance in the helical and spiral coils.

Researches have been done relating to increase in the range of wireless power transfer and the efficiency [5, 18]. For the cases like medical implants, where the size of transmitter coil and receiver coil are considerably different, the combination of near field and far field modes is suitable for optimal power transfer [19]. Resonant magnetic fields approach can be utilized to

investigate the detection schemes for changes in conductivity and permittivity of given solution salt water solution in [9].

Use of 3- dimensional spiral coils as both transmitter and receiver both has been a general trend since the days of rebirth of WPT . However, use of PCB coils reduces the space for many applications, for instance, in medical implants. The size of coils is so designed that the coil system acts as magnetic dipoles for the frequencies of inductive WPT schemes where the excitation wavelength exceeds 10m. Considering this thing in mind, we have designed PCB coils exactly identical in shape and size by UV photo lithography, where shape design was made using Target 3001! V15 Light software. PCB coils offer a highly scalable geometry for WPT through strongly coupled inductive resonators and can be designed to have high Q-factors with strong coupling over significant distances [24].

Methods have been investigated to increase the wireless power transfer [5,6,12]. These include the use of magnetic super-lens and meta-materials. In [12], it is shown with numerical simulations that the WPT efficiency increased from 48% without using to 72% with using Perfect Magnetic Conductors, PMCs.

1.2 Current Status of Wireless Power : A Brief Summary

Today, after around seven years since the rebirth of research in this field, commercially no products can be seen in the market: at least not using magnetic resonance or that which can transfer the power over a significant distance. The researchers at Massachusetts Institute of Technology (MIT) involved in this project started a company, WiTricity, to commercialize their discovery. Their primary targets are Original Equipment Manufacturers (OEM's) that can embed their technology directly into their products. But no such products have been released yet. They have their four own products, all using magnetic resonance [2]. Three of them are low power development kits aimed to showcase the technology for developers. The fourth one is a high power system for charging electrical cars. The products that are starting to pop up are charge pads/mats most of them uses the Qi standard which is created by the Wireless Power Consortium [3], WPC. Qi (is a Chinese word with meaning "energy flow" and pronounced as "Chee") is an interface standard developed by WPC for inductive electrical power transfer. [20]. The Qi system comprises a power transmission pad and a compatible

receiver in a portable device. To use the system, the mobile device is placed on top of the power transmission pad, which charges it via resonant inductive coupling. The WPC consists of over 140 members including industry leaders in mobile phones, batteries and consumer electronics. Their Qi standard is made for low power wireless charging, < 5W, and it specifies coil geometries, frequencies, communication, control and electric sources. The standard enables some design freedoms and is said to work with both direct induction and magnetic resonance. Most products today use the first technique and the maximum transfer distance for a Qi product today is 4cm. The WPC are working on a standard for medium power < 120W, but the specification for that is not made public yet. Their goal is to make worldwide standards for wireless power which is compatible for all devices, similar to Wi-Fi. Many of the large companies are doing their own research in this area e.g. Apple, Qual- comm, Duracell and Texas Instrument, Mitsubishi Electric Research Laboratories etc. Imura et al studied power transfer characteristics of resonance coils that fit the Electric Vehicles (EV)[4]. They showed from the experiment that there are two resonance frequencies at small separation of coils whereby the efficiency is maximum. And at larger separation, the efficiency is slightly decreased and considered power is transferred to the receiving coil although the coupling was significantly reduced.

The technologies based on magnetic coupling are less sensitive to surrounding objects and they do not have hazardous biological effects, and are more suitable for the increasing demands of wireless charging of electronic devices. The use of wireless technology would be proved to be beneficial if the efficiency of these systems is at least comparable to that of wired technology. The fear of efficiency of these chargers will be wiped out when a global mid-range-wireless standard is implemented [2]. Then all devices will not need to have its own charger, which in turn will save a lot of resources and energy. Another benefit is in the battery area: sensors, remotes etc could run without batteries and phones, tablets etc could be fitted with smaller ones because they would be charged in many places. Decreasing the need for batteries will have a huge effect on the environment because of the reduction of hazardous materials they use.

If one gazes to the social aspect, on the other hand, it is more than obvious that people, especially young ones, carry their chargers with them most of the time. With the development of universal mid-range-wireless systems, this burden will be removed since there could be charge zones in relevant areas like coffee shops, class rooms, parking places to fulfill the charging need.

Broadly speaking, three methods can be attributed to WPT: radiant WPT technology, inductive coupling WPT technology and resonant coupling WPT technology. The transfer of the electromagnetic waves goes to radiant WPT technology and could be widely applied in space transfer and satellite solar power station. Inductive coupling WPT technology, has been in use, is effective for very short distances [5][6]. Resonant Coupling WPT is based on magnetic resonance theory and is non-radiant transfer process where the transfer distance is few times the coil dimension [1].

A chart of the wireless power transfer methods [23] is presented as under:

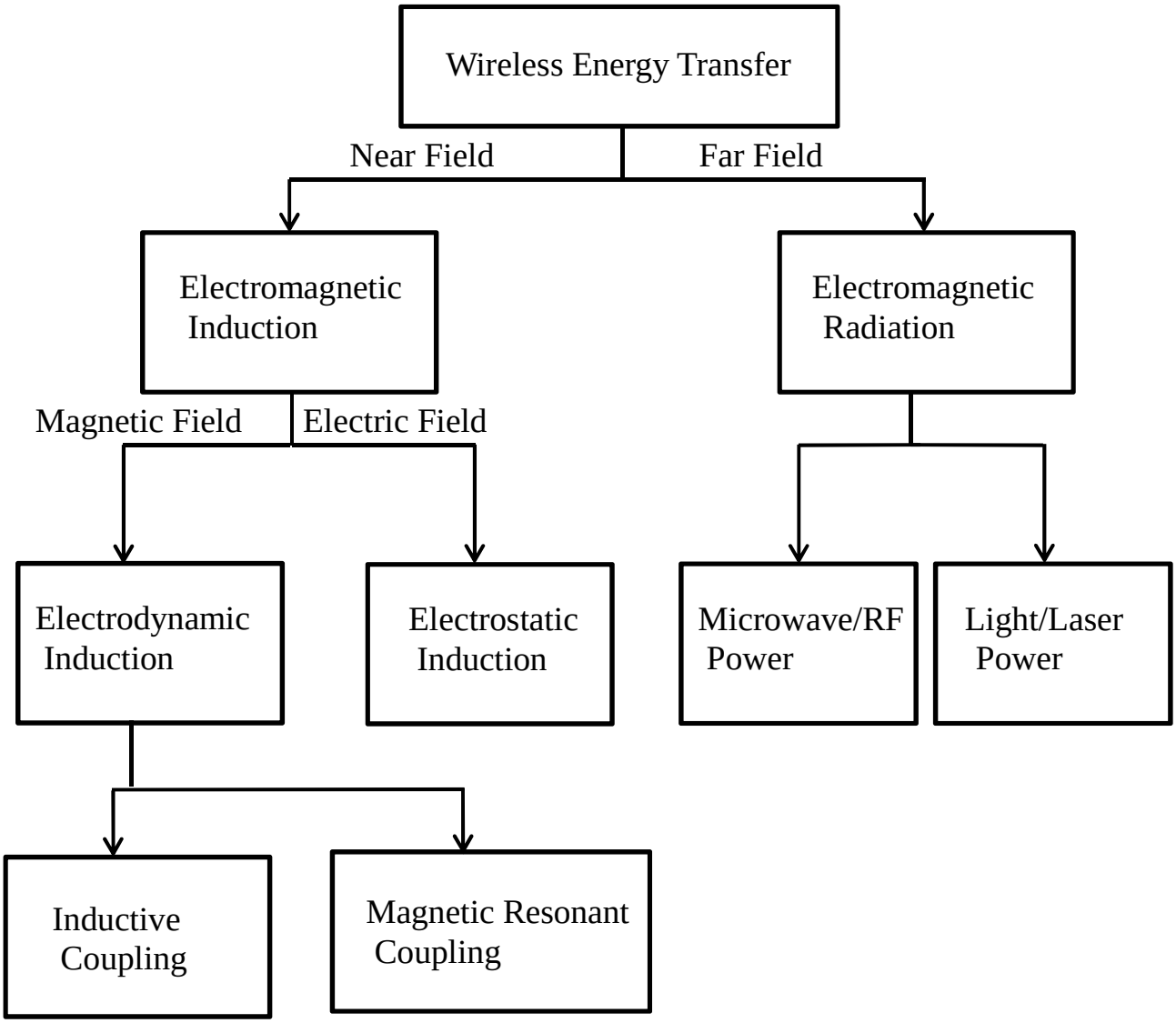

Table1.1: chart of power transfer schemes

1.3 Outline of thesis

The outline of this thesis will be as follows:

Chapter 2 will be presented with the basic theories of resistance, resonance and Q-factor, self-inductance, mutual induction and dipole approximation.

Chapter 3 contains coupled mode theory and experimental part of the project.

In chapter 4, results obtained from our project and discussion of the results with analysis are presented.

Finally conclusion and recommendation for further work are included in chapter 5 following the references and Appendix.

Chapter 2: Basics of Electromagnetism

The basic theory of electromagnetism is thought to be relevant for the thesis. So, the topics like *Resistance and Skin Depth, Self/Mutual Inductance, Mutual Inductances of Two Coils and Dipole Approximation, Maxwell's Equations* and *Potentials* are presented.

2.1 Resistance and Skin Depth

The dc resistance or the resistance of a wire (i.e. resistance at low frequencies) can be written in terms of resistivity ρ of the material of wire, its length *l* and area of cross-section *A*

$$R_{dc} = \frac{\rho l}{A} \qquad (2.1)$$

When the frequency increases, the current distribution in a conductor also changes. It goes from uniform distribution over entire volume of conductor to limit on the surface only. Skin depth δ is the measure of how the change of current distribution occurs with change in frequency.

Skin depth is defined as the depth from the outer surface of the conductor to a point where the current density falls to $1/e$ (i.e. about 37 %) of its value at the surface. Mathematically, it is given by:

$$\delta = 2\rho r\omega\mu \qquad (2.2)$$

where ω is the angular frequency and μ is the absolute magnetic permeability of the conductor and ρ is the resistivity of the material of conductor. Skin depth is the fundamental length scale for penetration currents and fields inside a conductor. [7]

2.2 Resonance and Q-value

The magnitude of transfer function when output is taken across resistor R of the LCR series circuit shown below can be written as[22]

$$|H(\omega)| = \left|\frac{V_0(\omega)}{V_i(\omega)}\right| = \frac{R}{Z} = \frac{R}{\sqrt{R^2+\left(\omega L-\frac{1}{\omega C}\right)^2}} = \frac{\omega CR}{\sqrt{\omega^2C^2R^2+(\omega^2LC-1)^2}}$$

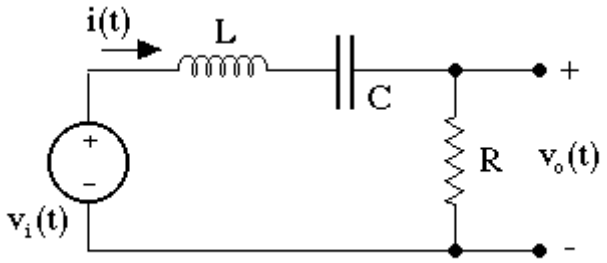

Figure(2.1): An LCR series circuit

$|H(\omega)| = 1$ corresponds to $\omega^2LC - 1 = 0$ or equivalently to $\omega = \omega_0 = \frac{1}{\sqrt{LC}}$.

This frequency which corresponds to maximum value of transfer function or, in other words, maximum output voltage is called resonance frequency. Physically, it is the frequency for which the oscillations of the total initial energy present in fully charged capacitor take place between the capacitor as electrical energy and inductor as magnetic energy . This frequency depends on parameters of the coil and capacitor, such as physical dimensions, positioning and fabrication materials, as well as geometry and the materials placed inside and nearby. Such effects could be utilized in detectors. A fluid level sensor based on detecting fluid level between two plates connected to a coil could be taken as an example where change in fluid level between the plates causes alter in the capacitance , leading to a shift in the resonance frequency.

The impedance of LCR series circuit is:

$$Z = \sqrt{R^2 + \left(\omega L - \frac{1}{\omega C}\right)^2}$$

At resonance, capacitive reactance is equal to the inductive reactance and the impedance is purely resistive.

The two points on both sides of resonance peak corresponding to which power drops to one half of the power corresponding to the resonance peak are called half power points. At these points, voltage drop across the resistor is $\frac{1}{\sqrt{2}}$ times the voltage drop across it at resonance. The frequency separation between these two points is called band width (BW).

$$\frac{1}{\sqrt{2}} = \frac{R}{\sqrt{R^2 + \left(\omega L - \frac{1}{\omega C}\right)^2}}$$

Squaring both sides,

$$\frac{1}{2} = \frac{R^2}{R^2 + \left(\omega L - \frac{1}{\omega C}\right)^2}$$

The roots of this equation can be shown to be:

$$\omega_1 = -\frac{R}{2L} + \sqrt{\left(\frac{R}{2L}\right)^2 + \frac{1}{\omega_0^2}}$$

$$\omega_2 = \frac{R}{2L} + \sqrt{\left(\frac{R}{2L}\right)^2 + \frac{1}{\omega_0^2}}$$

The bandwidth is, therefore,

$$\text{B}=\omega_2 - \omega_1 = \frac{R}{L}$$

This shows that bandwidth is proportional to the resistance in the circuit. So for resonance will be sharp for smaller values of R.

Multiplying above two expressions of $\omega_1$and ω_2, we obtain:

$$\omega_0 = \sqrt{\omega_1 \omega_2}$$

That means the resonance frequency of an LCR series circuit is the geometric mean of the half power frequencies.

Dissipative characteristics will start to dominate with increase of resistance in this frequency range. The sharpness of resonance peak is related to a quantity called *Quality Factor* (or *Q-factor*) which is defined as:

$$Q = \frac{Energy\ stored\ in\ the\ circuit}{Energy\ dissipated\ in\ the\ circuit} = \frac{\omega_0 L}{R}$$

This relation shows that the Q-factor of an LCR series circuit increases with decreasing the value of resistance, R and vice versa.

Q-factor expression can be written in terms of bandwidth B as

$$Q = \frac{\omega_0}{B}$$

The relation is, thus, inverse in between Q-factor and bandwidth. That means for the increase in Q-factor reduces the bandwidth of the circuit.

2.3 Self-Inductance

Magnetic flux linked through an isolated circuit due to variation of current in the circuit itself depends on geometry of the circuit. For a rigid stationary circuit, flux Φ changes due to the change in current I[8]:

$$\frac{\mathrm{d}\Phi}{dt} = \frac{\mathrm{d}\Phi}{dI}\frac{\mathrm{d}I}{dt} \qquad (2.3)$$

The quantity $\frac{\mathrm{d}\Phi}{dI}$ i.e. the ratio of change in flux to the change in current is called self-inductance (L) of the circuit.

From faraday's law of Electromagnetic induction, the emf (voltage) induced in the circuit due change in current (and hence magnetic flux) through it is given by:

$$\mathcal{E} = -\frac{\mathrm{d}\Phi}{dt} = -\frac{\mathrm{d}\Phi}{dI}\frac{\mathrm{d}I}{dt} = -L\frac{\mathrm{d}I}{dt} \qquad (2.4)$$

2.4 Mutual Inductance

If there is another circuit in the neighborhood of a circuit, the flux in first circuit changes due to the variation of current in second circuit in addition to the current in itself. The ratio of change $d\Phi_{12}$ in flux linked in C_1 due to change dI_2 in current in circuit C_2 is called mutual inductance M_{12} between the circuits:

$$M_{12} = \frac{d\Phi_{12}}{dI_2} \qquad (2.5)$$

We can find Neumann's formula for mutual inductance by taking into account of two coaxial circular coils each of radius '*a*' their axis is being taken along z-direction, without loss of generality. The position vectors of current elements $I_1 d\boldsymbol{l}_1$ and $I_2 d\boldsymbol{l}_2$ are $\boldsymbol{r}_1$ and $\boldsymbol{r}_2$ respectively from arbitrary origin O as shown in figure.

Total flux linked with loop C_1 due to constant current I_2 flowing through loop C_2 is given by:

$$\Phi_{12} = \int B_2 . d\boldsymbol{s}_1 = \int [\nabla \times A_2] . d\boldsymbol{s}_1 = \frac{\mu_0 I_2}{4\pi} \int \left[\nabla \times \oint \frac{d\boldsymbol{l}_2}{|\boldsymbol{r}_2 - \boldsymbol{r}_1|} \right] . d\boldsymbol{s}_1 \qquad (2.6)$$

Here integral is taken over a surface S_1 enclosed by loop C_1 to sum up the small fluxes through area elements of the surface considered and the line integral is taken over the closed loop C_2 so that the magnetic vector potential at any point on loop C_1 is due to whole loop C_2. The vector differential operator ∇ represents the differentiation with respect to field coordinates.

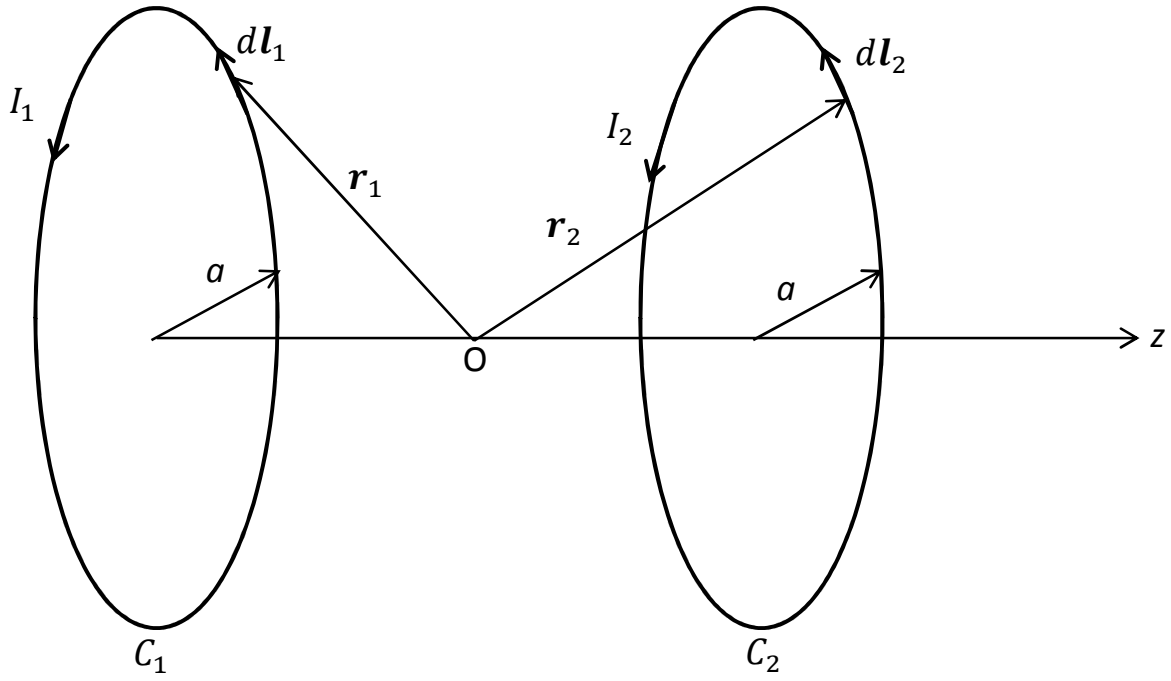

Figure 2.2[9]: Coaxial circular current loops for finding Neumann's formula for Mutual Inductance.

Since integration is taken over source coordinates, we can interchange the position of curl and line integral:

$$\Phi_{12} = \frac{\mu_0 I_2}{4\pi} \int \left[\oint \nabla \times \frac{d\boldsymbol{l}_2}{|\boldsymbol{r}_2 - \boldsymbol{r}_1|} \right] . d\boldsymbol{s}_1 \qquad (2.7)$$

We can convert the surface integral into line integral using Stokes' Theorem of vector calculus [7] which states that for any well-behaved vector field $\boldsymbol{A}(\boldsymbol{r})$, the line integral taken over any closed curve C is equal to the integral over any open surface S bounded by curve C:

$$\oint \boldsymbol{A} . d\boldsymbol{l} = \int \nabla \times A . d\boldsymbol{a} \qquad (2.8)$$

So, for our case:

$$\Phi_{12} = \frac{\mu_0 I_2}{4\pi} \int \left[\oint \nabla \times \frac{d\boldsymbol{l}_2}{|\boldsymbol{r}_2 - \boldsymbol{r}_1|} \right] . d\boldsymbol{s}_1 = \frac{\mu_0 I_2}{4\pi} \oint \oint \frac{d\boldsymbol{l}_2 . d\boldsymbol{l}_1}{|\boldsymbol{r}_2 - \boldsymbol{r}_1|} \qquad (2.9)$$

Similarly two integrations are taken with respect to different variables. So, their positions can also be interchanged:

$$\Phi_{12} = \frac{\mu_0 I_2}{4\pi} \oint \oint \frac{d\boldsymbol{l}_1 . d\boldsymbol{l}_2}{|\boldsymbol{r}_2 - \boldsymbol{r}_1|} \qquad (2.10)$$

Finally, flux linked through loop C_1 changes due to change in current I_2 in loop C_2 so that we can differentiate above expression with respect to I_2 to get the mutual inductance M_{12}:

$$\mathrm{M}_{12} = \frac{\mathrm{d}\Phi_{12}}{dI_2} = \frac{\mu_0}{4\pi} \oint \oint \frac{d\boldsymbol{l}_1 . d\boldsymbol{l}_2}{|\boldsymbol{r}_2 - \boldsymbol{r}_1|} \qquad (2.11)$$

This expression represents *Neumann's formula* for Mutual Inductance.

If we follow the same steps for the variation of flux linked with C_2 due to change in current I_1 in C_1, we would get the same result:

$$\mathrm{M}_{21} = \frac{\mathrm{d}\Phi_{12}}{dI_2} = \frac{\mu_0}{4\pi} \oint \oint \frac{d\boldsymbol{l}_2 . d\boldsymbol{l}_1}{|\boldsymbol{r}_2 - \boldsymbol{r}_1|} = \frac{\mu_0}{4\pi} \oint \oint \frac{d\boldsymbol{l}_1 . d\boldsymbol{l}_2}{|\boldsymbol{r}_2 - \boldsymbol{r}_1|} \qquad (2.12)$$

This takes us to the conclusion that:

$$\mathrm{M}_{12} = \mathrm{M}_{21} = M \text{ (say)} \qquad (2.13)$$

We can directly write Neumann's formula for self-inductance as:

$$L = \frac{\mu_0}{4\pi} \oint \oint \frac{d\boldsymbol{l} . d\boldsymbol{l}'}{|\boldsymbol{r} - \boldsymbol{r}'|} \qquad (2.14)$$

The great care to be taken here is on the singularity at point $\boldsymbol{r} = \boldsymbol{r}'$.

2.5 Mutual inductance of two coils and dipole approximation

For the distances larger as compared to the coil dimensions, dipole approximation is used as is done by Kurs et al. The mutual inductance in such cases follows inverse cube law in distance. Here, for the sake of completeness, the derivation of this inverse cube formula of mutual inductance is presented [9].

If $\boldsymbol{r}_1$ and $\boldsymbol{r}_2$ represent position vectors of two line elements $d\boldsymbol{l}_1$ and $d\boldsymbol{l}_2$ (or the current elements $I_1 d\boldsymbol{l}_1$ and $I_2 d\boldsymbol{l}_2$) respectively of two coils C_1 and C_2 which are at a distance r apart, use of Neumann's formula for the mutual inductance between the coils reads:

$$M \approx \frac{\mu_0}{4\pi r} \oint \oint d\boldsymbol{l}_1 . d\boldsymbol{l}_2 + \frac{\mu_0}{4\pi r^3} \oint \oint (d\boldsymbol{l}_1 . d\boldsymbol{l}_2)(\boldsymbol{r}_1 . \boldsymbol{r}_2) \qquad (2.15)$$

First term, that represents monopole contribution to Mutual Inductance, can be shown to vanish.

The remaining term can be written as:

$$M \approx \frac{\mu_0}{4\pi r^3} \oint d\boldsymbol{l}_2 \,.\, [\oint d\boldsymbol{l}_1 (\boldsymbol{r}_1 . \boldsymbol{r}_2)] \qquad (2.16)$$

Use of vector triple product of the form $\boldsymbol{a} \times (\boldsymbol{b} \times \boldsymbol{c}) = \boldsymbol{b}(\boldsymbol{a}.\boldsymbol{c}) - \boldsymbol{c}(\boldsymbol{a}.\boldsymbol{b})$ in the integrand of above equation, changes it to:

$$d\boldsymbol{l}_1 (\boldsymbol{r}_1 . \boldsymbol{r}_2) = \boldsymbol{r}_1 (\boldsymbol{r}_2 . d\boldsymbol{l}_1) - \boldsymbol{r}_2 \times (\boldsymbol{r}_1 \times d\boldsymbol{l}_1) \qquad (2.17)$$

First term in *RHS* involves multiplication across the loop, and needs some modification:

Consider the term $\boldsymbol{r}_1 (\boldsymbol{r}_1 . \boldsymbol{r}_2)$ and differentiate it w. r. to $\boldsymbol{r}_1$ taking into consideration of the fact that $d\boldsymbol{l}_1 = d\boldsymbol{r}_1$ since $\boldsymbol{r}_1$ changes along the loop:

$$d[\boldsymbol{r}_1 (\boldsymbol{r}_1 . \boldsymbol{r}_2)] = d\boldsymbol{r}_1 (\boldsymbol{r}_1 . \boldsymbol{r}_2) + \boldsymbol{r}_1 (d\boldsymbol{r}_1 . \boldsymbol{r}_2) = d\boldsymbol{r}_1 (\boldsymbol{r}_1 . \boldsymbol{r}_2) + \boldsymbol{r}_1 (d\boldsymbol{r}_1 . \boldsymbol{r}_2)$$

$$= d\boldsymbol{l}_1 (\boldsymbol{r}_1 . \boldsymbol{r}_2) + \boldsymbol{r}_1 (d\boldsymbol{l}_1 . \boldsymbol{r}_2)$$

$$\Longrightarrow \boldsymbol{r}_1 (d\boldsymbol{l}_1 . \boldsymbol{r}_2) = \boldsymbol{r}_1 (\boldsymbol{r}_2 . d\boldsymbol{l}_1) = d[\boldsymbol{r}_1 (\boldsymbol{r}_1 . \boldsymbol{r}_2)] - d\boldsymbol{l}_1 (\boldsymbol{r}_1 . \boldsymbol{r}_2) \qquad (2.18)$$

Substituting this in equation (2.17), we have,

$$d\boldsymbol{l}_1 (\boldsymbol{r}_1 . \boldsymbol{r}_2) = d[\boldsymbol{r}_1 (\boldsymbol{r}_1 . \boldsymbol{r}_2)] - d\boldsymbol{l}_1 (\boldsymbol{r}_1 . \boldsymbol{r}_2) - \boldsymbol{r}_2 \times (\boldsymbol{r}_1 \times d\boldsymbol{l}_1)$$

$$\Rightarrow d\boldsymbol{l}_1 (\boldsymbol{r}_1 . \boldsymbol{r}_2) = \frac{1}{2} d[\boldsymbol{r}_1 (\boldsymbol{r}_1 . \boldsymbol{r}_2)] - \frac{1}{2} [\boldsymbol{r}_2 \times (\boldsymbol{r}_1 \times d\boldsymbol{l}_1)] \qquad (2.19)$$

With this, the mutual inductance expression assumes the form:

$$M \approx \frac{\mu_0}{4\pi r^3} \oint d\boldsymbol{l}_2 \,.\, \left[\oint \left\{\frac{1}{2} d[\boldsymbol{r}_1 (\boldsymbol{r}_1 . \boldsymbol{r}_2)] - \frac{1}{2} [\boldsymbol{r}_2 \times (\boldsymbol{r}_1 \times d\boldsymbol{l}_1)]\right\}\right] \qquad (2.20)$$

Here first integral inside braces vanishes since the integral (integral being taken over closed curve $\mathbf{C}_1$) of differentiation over a closed curve is zero.

Thus,

$$M \approx \frac{\mu_0}{4\pi r^3} \oint d\boldsymbol{l}_2 \,.\, \left[\oint \frac{1}{2} [(\boldsymbol{r}_1 \times d\boldsymbol{l}_1)]\right] \times \boldsymbol{r}_2 \qquad (2.21)$$

The vector $\boldsymbol{r}_1 \times d\boldsymbol{l}_1$ has two components: one along the axis, with magnitude equal to the radius of R the loop and the other towards centre which is equal in magnitude but opposite in

sign for every opposite pairs of $d\boldsymbol{l}_1$elements thereby cancelling one another. So only axial component will contribute to the integral yielding:

$$\oint \frac{1}{2}(\boldsymbol{r}_1 \times d\boldsymbol{l}_1) = \oint \frac{1}{2} R\boldsymbol{e}_{s_1} d\boldsymbol{l}_1 = \frac{1}{2} R\boldsymbol{e}_{s_1} \oint d\boldsymbol{l}_1 = \frac{1}{2} R\boldsymbol{e}_{s_1} * 2\pi R = \pi R^2 \boldsymbol{e}_{s_1} = S_1 \boldsymbol{e}_{s_1} = \boldsymbol{S}_1$$

where $\boldsymbol{e}_{s_1}$ is unit vector along the axis of coil 1 and is normal to its loop area S_1.

Similarly, $\oint \frac{1}{2}(\boldsymbol{r}_2 \times d\boldsymbol{l_2}) = S_2 \boldsymbol{e}_{s_2} = \boldsymbol{S}_2$ represents area vector of coil 2.

The mutual inductance expression then takes the form:

$$M \approx \frac{\mu_0}{4\pi r^3} \oint d\boldsymbol{l}_2 . (\boldsymbol{S}_1 \times \boldsymbol{r}_2) = \frac{\mu_0}{4\pi r^3} \oint \boldsymbol{S}_1 . (\boldsymbol{r}_2 \times d\boldsymbol{l}_2) \qquad (2.22)$$

where use have been made of box product of three vectors.

Above expression can be written as:

$$M \approx \frac{\mu_0}{4\pi r^3} \oint \boldsymbol{S}_1 . (\boldsymbol{r}_2 \times d\boldsymbol{l}_2) = \frac{\mu_0}{4\pi r^3} \boldsymbol{S}_1 . \oint (\boldsymbol{r}_2 \times d\boldsymbol{l}_2)$$

$$= \frac{\mu_0}{4\pi r^3} \boldsymbol{S}_1 . 2\boldsymbol{S}_2 = \frac{\mu_0 \boldsymbol{S}_1 . \boldsymbol{S}_2}{2\pi r^3} = \frac{\mu_0}{2\pi} \frac{S_1 S_2 cos\theta}{r^3} \qquad (2.23)$$

For given orientation of coils (i.e. θ fixed), we can write:

$$M = \frac{Constant}{r^3} \qquad (2.24)$$

Above relation reveals that the mutual inductance of given pair of coils will be maximum at a given distance only when the coils are completely aligned (i.e., when angle between the axes of the coils equals to 0^o).

2.6 Displacement Current and Maxwell's Equations

The set of partial differential equations assembled, first, by Scottish Physicist James Clerk Maxwell in 1860's after suitable change in *Ampere's Circuital Law* are famous as *Maxwell's Equations*. This set of equations explains, mathematically, how the electric and magnetic fields vary due to variation in current and charge densities, and also the variation of these fields with respect to each other. Maxwell made modification in *Ampere's Circuital Law* by

introducing the concept of displacement current, $\boldsymbol{D}$. How this modification was done is given as under.

Displacement current is the keystone of Maxwell's electromagnetic theory [8] and plays its role in the topics like Optics, Relativity, and Waves etc besides electromagnetic theory. Integral form of Ampere's circuital law states that the line integral of magnetic field $\boldsymbol{B}$ around a closed loop is proportional to the conduction current enclosed by the loop:

$$\oint \boldsymbol{B}.d\boldsymbol{l} = \mu_0 I \tag{2.25}$$

For a current density *J*, the current *I* can be written as:

$$I = \iint \boldsymbol{J}.d\boldsymbol{a} \tag{2.26}$$

Line integral on left hand side of eq. (2.25) can be converted to surface integral using Stokes' theorem:

$$\oint \boldsymbol{B}.d\boldsymbol{l} = \iint (\boldsymbol{\nabla} \times \boldsymbol{B}).d\boldsymbol{a} \tag{2.27}$$

Combining equations (2.25), (2.26) and (2.27), we obtain:

$$\boldsymbol{\nabla} \times \boldsymbol{B} = \mu_0 \boldsymbol{J} \tag{2.28}$$

This is differential form of *Ampere's Circuital Law* and is valid for static current.

Faraday's law of electromagnetic induction relates the emf, $\oint \boldsymbol{E}.d\boldsymbol{l}$, induced across two ends of a conductor, moving in a magnetic field, with the rate of change of magnetic flux, $\iint \boldsymbol{B}.d\boldsymbol{a}$, linked with the conductor:

$$\oint \boldsymbol{E}.d\boldsymbol{l} = -\frac{\partial}{\partial t}\iint \boldsymbol{B}.d\boldsymbol{a} \tag{2.29}$$

Using Stokes' theorem in left hand side of this equation, we will have surface integral in both sides and the equation will be converted to the differential form:

$$\nabla \times \boldsymbol{E} = -\frac{\partial \boldsymbol{B}}{\partial t} \tag{2.30}$$

To see that changing electric field produces magnetic field eq. (2.25), and hence eq. (2.28), needs some modification such that it contains some time varying term . This will reflect symmetry between $\boldsymbol{E}$ and $\boldsymbol{B}$ fields.

To see how a time-varying electric field creates magnetic fields, consider a capacitor which being charged. With the lapse of time during charging, the charge on capacitor plates goes on increasing. So electric field between the plates also increases. To calculate the field due to conduction current, let's have a look on the loop C in figure (2.2).

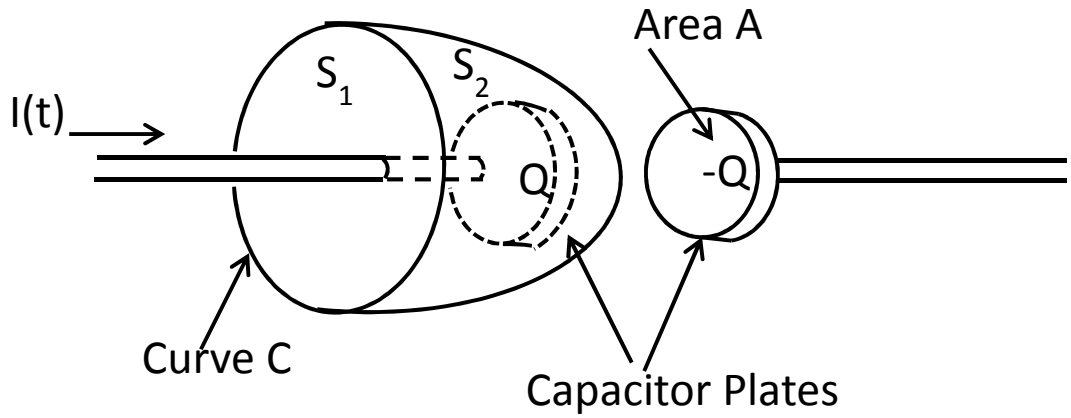

Figure (2.3): Testing *Ampere's Circuital Law*, showing loop C that bounds surfaces S_1 and S_2.

It is clear that the surface S_1 encloses the current I . Whereas current enclosed by S_2 the is 0. Hence, there seems an ambiguity in choosing the appropriate surface bounded by the loop C. This ambiguity was resolved by Maxwell by adding to the right-hand side of the Ampere's law an extra term, $\boldsymbol{J}_d = \epsilon_0 \frac{\partial \boldsymbol{E}}{\partial t} = \frac{\partial \boldsymbol{D}}{\partial t}$ called "Displacement Current". Here $\boldsymbol{D}$ is the electric displacement vector.

Thus the generalized Ampere's (or the Ampere-Maxwell) law can now be written as:

$$\boldsymbol{\nabla} \times \boldsymbol{B} = \mu_0(\boldsymbol{J} + \boldsymbol{J_d}) = \mu_0 \left(\boldsymbol{J} + \frac{\partial \boldsymbol{D}}{\partial t}\right) \qquad (2.31)$$

Equivalently,

$$\boldsymbol{\nabla} \times \boldsymbol{H} = (\boldsymbol{J} + \boldsymbol{J_d}) = \boldsymbol{J} + \frac{\partial \boldsymbol{D}}{\partial t} \qquad (2.32)$$

With the introduction of *Displacement Current*, the four basic equations of electricity and magnetism can be written collectively as:

$\boldsymbol{\nabla} \times \boldsymbol{B} = \mu_0 \left(\boldsymbol{J} + \frac{\partial \boldsymbol{D}}{\partial t}\right)$ [Ampere-Maxwell Law]

$\boldsymbol{\nabla} \times \boldsymbol{E} = -\frac{\partial \boldsymbol{B}}{\partial t}$ [Faraday's Law of Electromagnetic Induction]

$$\boldsymbol{\nabla}.\boldsymbol{E} = \rho/\epsilon_0 \qquad \text{[Gauss' law in Electrostatics]}$$

$$\boldsymbol{\nabla}.\boldsymbol{B} = 0 \qquad \text{[Gauss' law in Magnetism]}$$

These four equations are collectively known as Maxwell's equations.

2.7 Potentials

Various components of electric and magnetic fields are related through a set of coupled first-order differential equations. It is convenient to introduce potentials to get a smaller number (i.e. two) of second order differential equations.

Since divergence of magnetic field (***B***) is zero, it can be written in terms of vector potential, ***A***:

$$\boldsymbol{B} = \nabla \times \boldsymbol{A}$$

Using this equation in *Faraday's Law of Electromagnetic Field*:

$\nabla \times \boldsymbol{E} + \frac{\partial \boldsymbol{B}}{\partial t} = 0$, we obtain:

$$\nabla \times \left(\boldsymbol{E} + \frac{\partial \boldsymbol{A}}{\partial t}\right) = 0$$

The quantity within braces is, therefore, curl free. So, it can be written as the gradient of some scalar function, called scalar potential:

$$\boldsymbol{E} + \frac{\partial \boldsymbol{A}}{\partial t} = -\nabla\Phi \qquad (2.33)$$

So, $$\boldsymbol{E} = -\frac{\partial \boldsymbol{A}}{\partial t} - \nabla\Phi \qquad (2.34)$$

The ***E***- and ***B***-fields so defined in terms of vector and scalar potentials upon substitution on inhomogeneous Maxwell's equations would give:

$$\nabla^2\Phi + \frac{\partial(\nabla.\boldsymbol{A})}{\partial t} = -\rho/\epsilon_0 \qquad (2.35)$$

And $$\nabla^2\boldsymbol{A} - \frac{1}{c^2}\frac{\partial^2 \mathbf{A}}{\partial t^2} - \nabla\left(\nabla.\boldsymbol{A} + \frac{1}{c^2}\frac{\partial\Phi}{\partial t}\right) = -\mu_0\boldsymbol{J} \qquad (2.36)$$

Still we have coupled equations even though the number of differential equations is reduced. To uncouple them, we choose a set of potentials ($\boldsymbol{A}$, Φ) such that

$$\nabla.\boldsymbol{A} + \frac{1}{c^2}\frac{\partial \Phi}{\partial t} = 0 \tag{2.37}$$

Such a choice is referred to as *Lorentz gauge*. Thus we have:

$$\nabla^2\Phi + \frac{1}{c^2}\frac{\partial^2 \Phi}{\partial t^2} = -\rho/\epsilon_0 \tag{2.38}$$

$$\nabla^2\boldsymbol{A} - \frac{1}{c^2}\frac{\partial^2 \mathbf{A}}{\partial t^2} = -\mu_0\boldsymbol{J} \tag{2.39}$$

These two equations along with Lorentz gauge form a set of equations equivalent to Maxwell's equations in all respects. [7]

The solution of these equations can be written as:

$$\Phi(\boldsymbol{r}, \mathrm{t}) = \frac{1}{4\pi\epsilon_0}\int \frac{\rho\left(\mathbf{r}', t - \frac{|\boldsymbol{r}-\mathbf{r}'|}{c}\right)}{|\boldsymbol{r}-\mathbf{r}'|} d\tau' \tag{2.40}$$

$$\boldsymbol{A}(\boldsymbol{r}, \mathrm{t}) = \frac{1}{4\pi\epsilon_0}\int \frac{\boldsymbol{J}\left(\mathbf{r}', t - \frac{|\boldsymbol{r}-\mathbf{r}'|}{c}\right)}{|\boldsymbol{r}-\mathbf{r}'|} d\tau' \tag{2.41}$$

The potentials so obtained are called retarded potentials since potential at a point is caused by the action of a source at a distance $|\boldsymbol{r} - \mathbf{r}'|$ away at an earlier or retarded time $\mathrm{t}' = t - \frac{|\boldsymbol{r}-\mathbf{r}'|}{c}$. The time difference $\frac{|\boldsymbol{r}-\mathbf{r}'|}{c}$ is just the time of propagation of disturbance from one point to another.

Chapter 3: Coupled Mode Theory and Experimental Set-up

3.1 Coupling of Modes

Coupled mode theory, CMT, is an analytic tool for systems involving interacting oscillations and leads to solutions for oscillating and propagating waves [11]. Therefore it is used to model wireless power system that uses magnetic resonance.

For an ideal LC circuit, the governing equations are two coupled fist order equations:

$$v = L\frac{di}{dt} \tag{3.1}$$

$$i = -C\frac{dv}{dt} \tag{3.2}$$

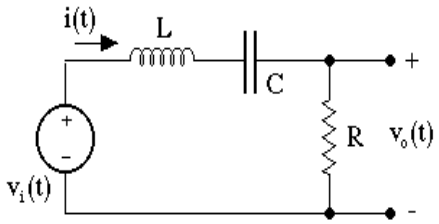

Figure (3.1): An *LC* circuit

From (3.1) and (3.2), we have:

$$v = L\frac{d}{dt}\left(-C\frac{dv}{dt}\right)$$

which on simplification gives:

$$\frac{d^2v}{dt^2} + \omega_0^2 v = 0 \tag{3.3}$$

Here, $\omega_0 = \sqrt{\frac{1}{LC}}$ is resonant angular frequency.¨

3.1.1 Properties of Coupled Equations:

Many systems in nature can be modeled using coupled first order differential equations. One example is an atom interacting with a laser pulse (resulting in Rabi oscillations), another example may include the interaction between two solenoids. Assume that one has two coupled equations of the form:

$$\frac{da_1}{dt} = j\omega_1 a_1 + \kappa_{12} a_2 \text{ and } \frac{da_2}{dt} = j\omega_2 a_2 + \kappa_{21} a_1 \tag{3.4}$$

Here a_1 and a_2 are the amplitudes of oscillations of system 1 and 2, respectively, while κ_{12} and κ_{21} are coupling coefficients between the two systems.

It is possible to write

$$\frac{d|a_1|^2}{dt} = \frac{d}{dt}(a_1 a_1^*) = a_1^* \frac{da_1}{dt} + a_1 \frac{da_1^*}{dt}$$

$$= a_1^*(j\omega_1 a_1 + \kappa_{12} a_2) + a_1(-j\omega_1 a_1^* + \kappa_{12}^* a_2^*) \tag{3.5}$$

which simplifies to:

$$\frac{d|a_1|^2}{dt} = \kappa_{12} a_1^* a_2 + \kappa_{12}^* a_2^* a_1 \tag{3.6}$$

In a similar fashion:

$$\frac{d|a_2|^2}{dt} = \kappa_{21} a_2^* a_1 + \kappa_{21}^* a_1^* a_2 \tag{3.7}$$

Adding (3.6) and (3.7) to obtain:

$$\frac{d|a_1|^2}{dt} + \frac{d|a_2|^2}{dt} = (\kappa_{12} + \kappa_{21}^*) a_1^* a_2 + (\kappa_{21} + \kappa_{12}^*) a_2^* a_1 \tag{3.8}$$

Conservation of energy (which is proportional to the square of amplitudes) requires that time rate of change of energy must vanish:

$$\frac{d|a_1|^2}{dt} + \frac{d|a_2|^2}{dt} = 0 \tag{3.9}$$

Since initial amplitudes and phases of a_1 and a_2 are arbitrary, we must have:

$\kappa_{12} + \kappa_{21}^* = 0$ and $\kappa_{21} + \kappa_{12}^* = 0$ for the condition (6) to be valid.

Thus we get:

$$\kappa_{12} = -\kappa_{21}^* \quad \text{and} \quad \kappa_{21} = -\kappa_{12}^* \tag{3.10}$$

Assume that $|\kappa_{12}| = |\kappa_{21}| = \kappa$ and that $a_1 = a_{10}e^{i\omega t}$ and $a_2 = a_{20}e^{i\omega t}$.

Substituting these values of a_1 and a_2 in (3.1):

$$j\omega a_1 = j\omega_1 a_1 + \kappa_{12} a_2 \tag{3.11}$$

$$j\omega a_2 = j\omega_2 a_2 + \kappa_{21} a_1 = j\omega_2 a_2 - \kappa_{12}^* a_1 \tag{3.12}$$

Solving these two equations for ω, we get:

$$\omega = \frac{\omega_1+\omega_2}{2} \pm \sqrt{\left(\frac{\omega_1-\omega_2}{2}\right)^2 + |\kappa|^2} = \frac{\omega_1+\omega_2}{2} \pm \Omega \tag{3.13}$$

where,

$$\Omega = \sqrt{\left(\frac{\omega_1-\omega_2}{2}\right)^2 + |\kappa|^2} \tag{3.14}$$

The most general solution of Eqn. (3.4) is:

$$a_1(t) = Ae^{j\left(\frac{\omega_1+\omega_2}{2}+\Omega\right)t} + Be^{j\left(\frac{\omega_1+\omega_2}{2}-\Omega\right)t} \tag{3.15}$$

$$a_2(t) = Ce^{j\left(\frac{\omega_1+\omega_2}{2}+\Omega\right)t} + De^{j\left(\frac{\omega_1+\omega_2}{2}-\Omega\right)t} \tag{3.16}$$

The constants A, B, C and D can be determined by assuming the initial conditions:

$a_1(t=0) = 0$ and $a_2(t=0) = a_2(0)$.

So, $A + B = 0 \Longrightarrow A = -B$ and $C + D = a_2(0)$

Again

$$\frac{da_1(t)}{dt} = Aj\left(\frac{\omega_1+\omega_2}{2} + \Omega\right)e^{j\left(\frac{\omega_1+\omega_2}{2}+\Omega\right)t} + Bj\left(\frac{\omega_1+\omega_2}{2} - \Omega\right)e^{j\left(\frac{\omega_1+\omega_2}{2}-\Omega\right)t} = j\omega_1 a_1 + \kappa_{12} a_2$$

And

$$\frac{da_2(t)}{dt} = Cj\left(\frac{\omega_1+\omega_2}{2}+\Omega\right)e^{j\left(\frac{\omega_1+\omega_2}{2}+\Omega\right)t} + Dj\left(\frac{\omega_1+\omega_2}{2}-\Omega\right)e^{j\left(\frac{\omega_1+\omega_2}{2}-\Omega\right)t} = j\omega_2 a_2 + \kappa_{21}a_1$$

Applying initial conditions to these expressions, we obtain:

$$Aj\left(\frac{\omega_1+\omega_2}{2}+\Omega\right) + Bj\left(\frac{\omega_1+\omega_2}{2}-\Omega\right) = \kappa_{12}a_2(0)$$

or, $$-Bj\left(\frac{\omega_1+\omega_2}{2}+\Omega\right) + Bj\left(\frac{\omega_1+\omega_2}{2}-\Omega\right) = \kappa_{12}a_2(0)$$

or, $$B = j\frac{\kappa_{12}}{2\Omega}a_2(0) = -A \qquad (3.17)$$

And, $$Cj\left(\frac{\omega_1+\omega_2}{2}+\Omega\right) + Dj\left(\frac{\omega_1+\omega_2}{2}-\Omega\right) = j\omega_2 a_2(0)$$

$$[a_2(0)-D]j\left(\frac{\omega_1+\omega_2}{2}+\Omega\right) + Dj\left(\frac{\omega_1+\omega_2}{2}-\Omega\right) = j\omega_2 a_2(0)$$

$$D = a_2(0)\frac{\left(-\frac{\omega_2-\omega_1}{2}+\Omega\right)}{2\Omega} \text{ and } C = a_2(0)\frac{\left(\frac{\omega_2-\omega_1}{2}+\Omega\right)}{2\Omega} \qquad (3.18)$$

With these constants, the solutions $a_1(t)$ and $a_2(t)$ take the form:

$$a_1(t) = -j\frac{\kappa_{12}}{2\Omega}a_2(0)e^{j\left(\frac{\omega_1+\omega_2}{2}+\Omega\right)t} + j\frac{\kappa_{12}}{2\Omega}a_2(0)e^{j\left(\frac{\omega_1+\omega_2}{2}-\Omega\right)t}$$

or, $$a_1(t) = a_2(0)\frac{\kappa_{12}}{\Omega}e^{j\frac{\omega_1+\omega_2}{2}t}sin\Omega t \qquad (3.19)$$

And

$$a_2(t) = a_2(0)\frac{\left(\frac{\omega_2-\omega_1}{2}+\Omega\right)}{2\Omega}e^{j\left(\frac{\omega_1+\omega_2}{2}+\Omega\right)t} + a_2(0)\frac{\left(-\frac{\omega_2-\omega_1}{2}+\Omega\right)}{2\Omega}e^{j\left(\frac{\omega_1+\omega_2}{2}-\Omega\right)t}$$

or, $$a_2(t) = a_2(0)e^{j\frac{\omega_1+\omega_2}{2}t}\left(cos\Omega\mathrm{t} + \mathrm{j}\frac{\omega_2-\omega_1}{2\Omega}sin\Omega\mathrm{t}\right) \qquad (3.20)$$

For the case of $\omega_2 = \omega_1$, we observe that the solutions (3.19) and (3.207) are out of phase.

In case of weak coupling between the systems, $\kappa_{12} \ll \frac{\omega_1-\omega_2}{2}$ and $\Omega \approx \frac{\omega_1-\omega_2}{2}$. For such systems,

$$|a_1(t)|^2 = a_2^2(0)\left(\frac{\kappa_{12}}{\Omega}\right)^2 sin^2\Omega t \qquad (3.21)$$

And $|a_2(t)|^2 = a_2^2(0)(cos^2\Omega t + sin^2\Omega t) = a_2^2(0) = constant$ (3.22)

It is obvious from (3.18) that $|a_1(t)|^2 = 0$ when $\Omega t = 0$ i.e. when $t = 0$.

When $t = \pi/\Omega$, $|a_1(t)|^2 = a_2^2(0)\left(\frac{\kappa_{12}}{\Omega}\right)^2 \ll a_2^2(0)$

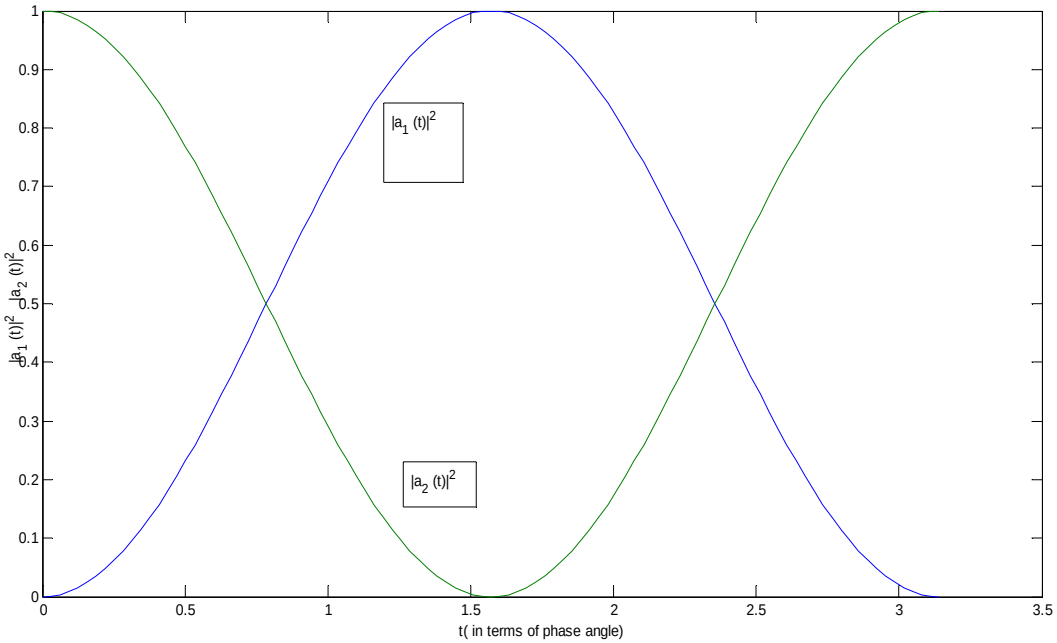

Figure (3.2): Energy in two coupled systems obtained using Matlab

3.1.2 Power Transfer in an LC Resonator

We need to determine the coupling coefficients in (1) to determine the power transfer between two systems in the figure below. Our aim is to find the formula used by Kurs et.al [4]

Assume that each system is a circuit that consists of a solenoid (L_1 in 1 and L_2 in 2) and a capacitor (C_1 in 1 and C_2 in 2). The mutual inductance between the coils is M which induces a voltage $M\,dI_1/dt$ in circuit 2 and $M\,dI_2/dt$ in circuit 1. If there is a dipolar coupling between the circuits, which is the case when distance D between the circuits is much larger than the size of each coil, we have $M = constant/D^3$. Assume, for the moment, neglible resistance($R_1 = R_2 = 0$).

The energy of circuit 1 is:

$$E_1 = \frac{1}{2}C_1V_{01}^2 = \frac{1}{2}L_1I_{01}^2 \tag{3.23}$$

where, $V_{01}$and I_{01} are voltage and current amplitudes.

Energy of circuit 2 is:

$$E_2 = \frac{1}{2}C_2V_{02}^2 = \frac{1}{2}L_2I_{02}^2 \tag{3.24}$$

where, V_{02} and I_{02} represent voltage and current amplitudes in circuit 2.

Let us now introduce new amplitudes as:

$$b_1 = \sqrt{\frac{1}{2}C_1}V_1 + j\sqrt{\frac{1}{2}L_1}I_1 \text{ and } b_2 = \sqrt{\frac{1}{2}C_2}V_2 + j\sqrt{\frac{1}{2}L_2}I_2 \tag{3.25}$$

where,

$$I_1 = \frac{1}{2}\left(I_{01}e^{j\omega_1 t} + I_{01}^*e^{-j\omega_1 t}\right) \tag{3.26}$$

and

$$I_2 = \frac{1}{2}\left(I_{02}e^{j\omega_2 t} + I_{02}^*e^{-j\omega_2 t}\right) \tag{3.27}$$

represent currents in circuits 1 and 2 respectively in complex form. Corresponding voltages are:

$$V_1 = \frac{1}{2}\left(V_{01}e^{j\omega_1 t} + V_{01}^*e^{-j\omega_1 t}\right) \tag{3.28}$$

And

$$V_2 = \frac{1}{2}\left(V_{02}e^{j\omega_2 t} + V_{02}^*e^{-j\omega_2 t}\right) \tag{3.29}$$

The square of modulus of the amplitude b_1 is:

$$|b_1|^2 = \frac{1}{2}L_1|I_1|^2 + \frac{1}{2}C_1|V_1|^2 \tag{3.30}$$

Taking time average (symbolized by angle brackets), we obtain:

$$\langle|b_1|^2\rangle = \frac{1}{4}L_1|I_{01}|^2 + \frac{1}{4}C_1|V_{01}|^2 \tag{3.31}$$

Here we have made use of:

$$\frac{1}{T}\int_0^T sin^2(\omega t)dt = \frac{1}{T}\int_0^T cos^2(\omega t)dt = \frac{1}{2}$$

(3.32)

Since both the inductance and capacitance must carry equal amounts of energy (averaged over one period), we have:

$$\langle|b_1|^2\rangle = \frac{1}{4}L_1|I_{01}|^2 + \frac{1}{4}C_1|V_{01}|^2 = \frac{1}{2}L_1|I_{01}|^2 = \frac{1}{2}C_1|V_{01}|^2 \quad (3.33)$$

Corresponding expression found for circuit 2 is:

$$\langle|b_2|^2\rangle = \frac{1}{4}L_2|I_{02}|^2 + \frac{1}{4}C_2|V_{02}|^2 = \frac{1}{2}L_2|I_{02}|^2 = \frac{1}{2}C_2|V_{02}|^2 \quad (3.34)$$

Using these observations, it is convenient to define new amplitudes a_1 and a_2 showing exponential time variation as:

$$a_1 = \sqrt{\frac{L_1}{2}}I_{01}e^{j\omega_1 t} \text{ and } a_2 = \sqrt{\frac{L_2}{2}}I_{02}e^{j\omega_2 t} \qquad (3.35)$$

which immediately result in

$$|a_1|^2 = \frac{L_1}{2}|I_{01}|^2 \text{ and } |a_2|^2 = \frac{L_2}{2}|I_{02}|^2 \qquad (3.36)$$

The amplitudes a_1 and a_2 have the same physical implications as those of Eq.(3.4) and therefore conclusions from section 1 also apply here.

The power transferred from circuit 1 to circuit 2 is given by:

$$P = \langle \mathcal{E}_M \mathrm{I}_M \rangle = \langle \mathrm{M}\frac{dI_1}{dt}\mathrm{I}_2 \rangle \qquad (3.37)$$

Here,

$$\frac{dI_1}{dt} = \frac{j\omega_1}{2}\left(I_{01}e^{j\omega_1 t} - I_{01}^* e^{-j\omega_1 t}\right) \qquad (3.38)$$

so that

$$P = \langle \mathrm{M}\frac{dI_1}{dt}\mathrm{I}_2 \rangle = M\,\langle\left[\frac{j\omega_1}{2}\left(I_{01}e^{j\omega_1 t} - I_{01}^* e^{-j\omega_1 t}\right)\right]\left[\frac{1}{2}\left(I_{02}e^{j\omega_2 t} + I_{02}^* e^{-j\omega_2 t}\right)\right]\rangle$$

or $$P = \frac{j\omega_1 M}{4}\langle\left[\left(I_{01}I_{02}^* e^{j(\omega_1-\omega_2)t} - I_{01}^* I_{02} e^{j(\omega_2-\omega_1)t}\right)\right]\rangle \qquad (3.39)$$

So, close to resonance, we have:

$$P = \frac{j\omega M}{2\sqrt{L_1 L_2}} \langle [(a_1^* a_2 - a_2^* a_1)] \rangle = \kappa_{12} a_1^* a_2 + \kappa_{12}^* a_2^* a_1 \qquad (3.40)$$

Comparing these expressions of power, we observe that

$$\kappa_{12} = -\kappa_{12}^* = \frac{j\omega M}{2\sqrt{L_1 L_2}} \qquad (3.41)$$

This equation together with $M = constant/r^3$, is used in figure 2 of [1].

3.1.3 Strong Coupling Regime

Taking into account the loss rates in addition to the exchange rates, the governing equations assume the form:

$$\frac{da_1}{dt} = (j\omega_1 - \Gamma_1)a_1 + \kappa_{12} a_2 \text{ and } \frac{da_2}{dt} = (j\omega_1 - \Gamma_1)a_2 + \kappa_{21} a_1$$

When two objects of same resonance frequency exchange energy at this frequency, the loss rates due to intrinsic absorption or radiative losses are to be minimal as compared to coupling rates to get perfect energy exchange. For this, the coupling coefficient should be greater than geometrical mean of resonant widths (i.e. loss rates) Γ_1, Γ_2:

$$\kappa \gg \sqrt{\Gamma_1 \Gamma_2}\ .$$

This regime (or the distance) over which this inequality holds is called strong coupling regime.

3.2 Frequency Splitting

At the distances greater than greatest size of the coils, efficiency peaks only at resonant frequency. However, efficiency peak appears at the positions both below and above the original resonant frequency if the coils are very close to each other. This is called frequency splitting.

3.3 Design of Printed Circuit Board (PCB) Coils and Photolithography

Photolithography is the process of transfer of geometric shapes on photo-mask (or simply mask) to a smooth surface, so called photo-resist, which is sensitive to light. Photo-resist is also called photopolymer. In between photo-resist and substrate (made of epoxy), there is a layer of copper.

Stepwise procedure for constructing coil is as follows:

- Coil shape and design is constructed using Target 3001! V15 Light software. The design is saved as file and is printed.
- Photocopy of this printed copy is taken in a transparency at two positions of the transparency so that after folding the two copies overlap to ensure good masking.
- Folded transparency is placed on the top of substrate after cleaning the substrate with Hydrogen Peroxide so as to remove contaminations, if any.
- Whole set up is placed inside the litho-meter and UV-Light is passed through the transparency for about half an hour.
- Removing the transparency, the photopolymer is developed using KOH solution. With this, the exposed portion of photopolymer will be washed away and that under the mask will remain.
- Applying ferric/ferrous chloride removes copper from the exposed portion. Lastly removing the photo-resist in the remaining will give the tracks of copper of given structure.

3.4 Measurements of Inductance and Inter-winding Capacitance

In addition to the measurements of inductance and inter-winding capacitance, the coil parameters were measured which are summarized in the table below.

Table 3.1: Measurement of Parameters of Coil

Coil type	Transmitting coil	Receiver coil
Outer radius	19.0mm	19.0mm
No. of turns	7	7

Turn width	2mm	2mm
Spacing between the turns	0.5mm	0.5mm

Replacing the capacitor of transmitting coil by a 47Ω resistor, data for pick-up voltage were taken to determine the resonant frequency of the receiving coil for two values of the capacitances. Thus we got two different values of resonant frequencies. This was done for finding the inter-winding capacitance. With capacitor of 2*nF*, the resonance frequency was found to be 17.25*MHz* whereas with the capacitor of 440*pF*, the resonance frequency was measured to be 19.33*MHz*. Then following formula was used to calculate the inter-winding capacitance and the inductor of the coil:

$$f_1 = \frac{1}{2\pi\sqrt{L(C_1+C_0)}}$$

$$17.25e6 = \frac{1}{2\pi\sqrt{L(2e-9+C_0)}}$$

and

$$f_2 = \frac{1}{2\pi\sqrt{L(C_2+C_0)}}$$

$$19.33e6 = \frac{1}{2\pi\sqrt{L(0.44e-9+C_0)}}$$

Solving these two equations, we get the values of L and C_0 to be:

$C_0 = 5.65nF$ and $L = 11nH$

3.5 Experimental Set-up

After designing two identical spiral PCB coils, two capacitors 2.2*nF* each are connected in series with the coils. The coils were attached to two oppositely faced Poly-Methyl Meth-Acrylate (PMMA) blocks which were fixed to movable stands on working board. One coil is connected to Agilent 33220A *Arbitrary Waveform Generator* that can produce signals of frequency up to 20 MHz. This coil, since transmits signals, is referred to as transmitter coil. The generator is set to output a sinusoidal wave. The frequency range we selected was from

10 MHz to 17MHz. The second coil, used as pick up coil, is connected to *Agilent 1002A Oscilloscope* to read the output voltage. The oscilloscope also reads voltage to the transmitting coil. To avoid the influence of external noise the whole experimental set up, except oscilloscope and signal generator, was spaced inside Faraday cage constructed in the Departmental Workshop, IFT, University of Bergen.

We can measure different parameters like peak-to-peak voltage, rms voltage, average voltage, peak voltage, phase/phase difference, minimum voltage etc for both pick-up and transmitter coils. We recorded the sampled values of instantaneous voltages in a USB as comma separated values files. The experiment was performed for the voltage variation with frequency and hence to find resonance frequency corresponding to the maximum pick-up voltage. Similarly variation of voltage with distance was performed near resonance frequency. At the same time on the screen, we have displayed Maximum values of excitation and pick-up voltages. These values were also noted with the variation in frequency (or distance between coils). The simple block diagram of the experimental set up is shown in figure(3.2) below

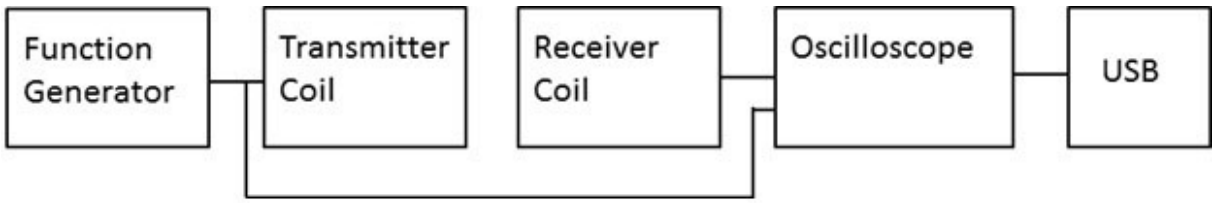

Figure (3.3): Block diagram of experimental set up for wireless power transfer system for our project

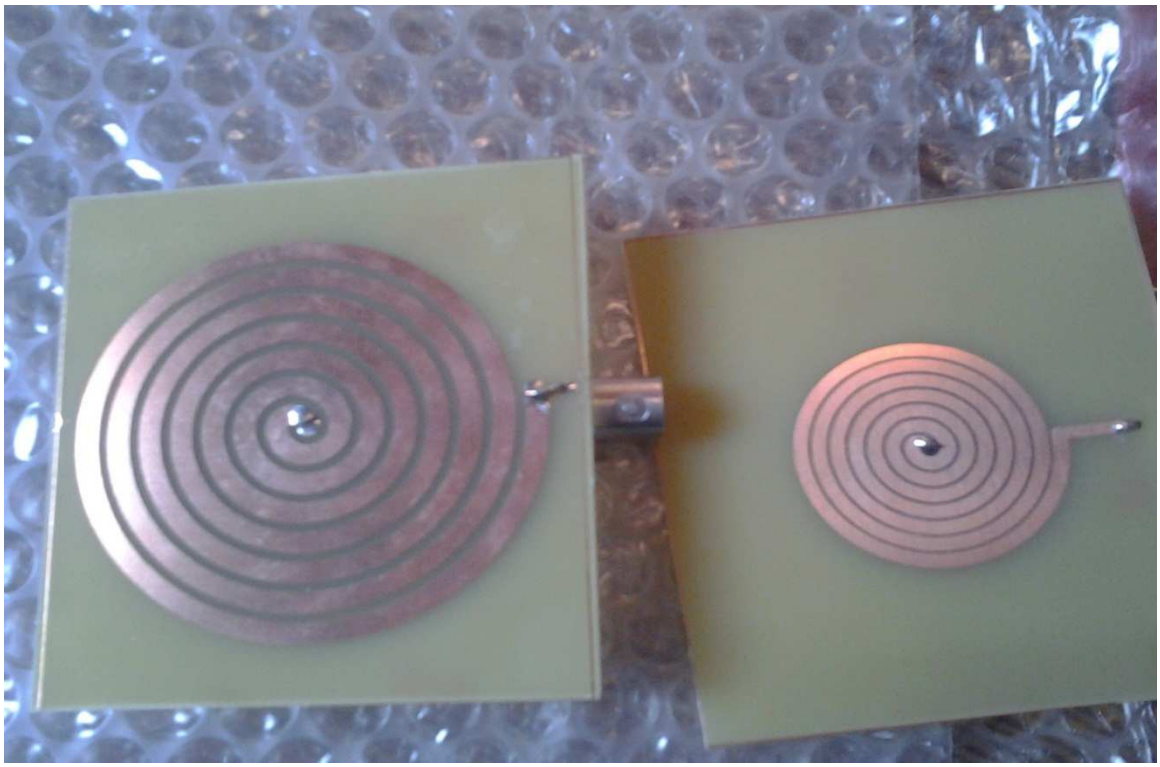

Figure (3.4): Two different sized coils designed using Light 3001! V15 software and photo lithography.

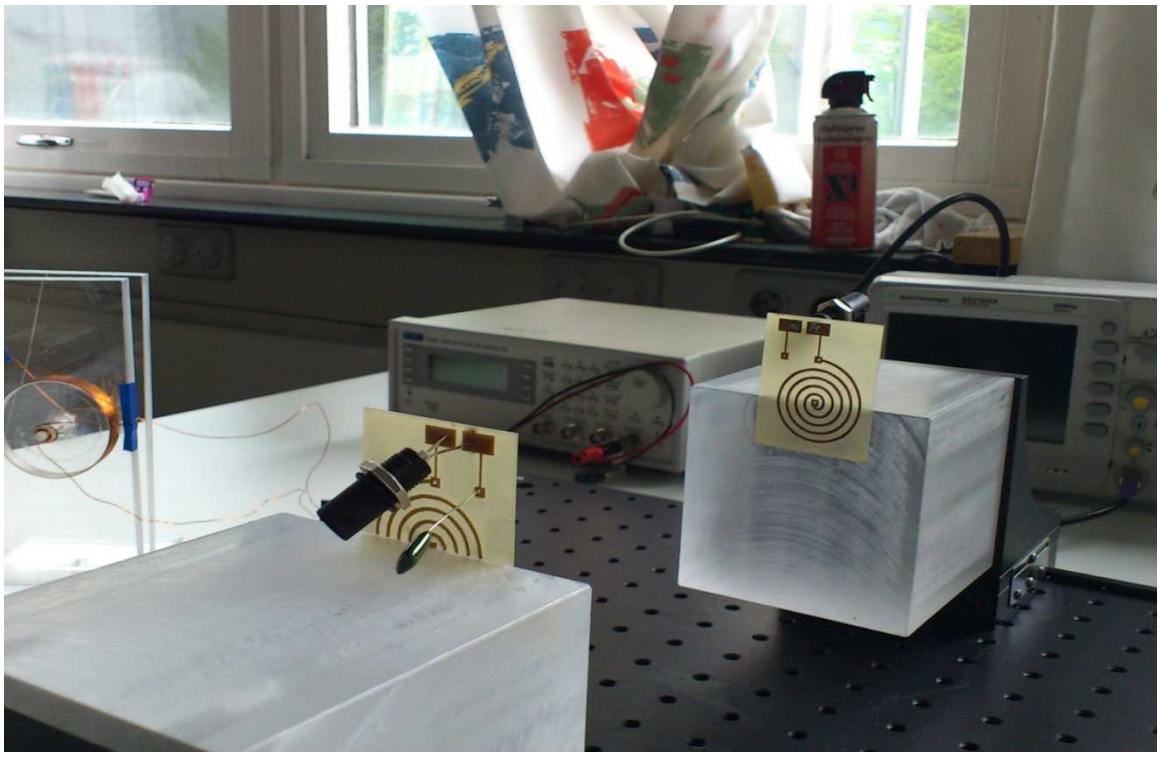

Figure (3.5): Showing two PMMA blocks to which PCB coils (which series combination with capacitors) are taped

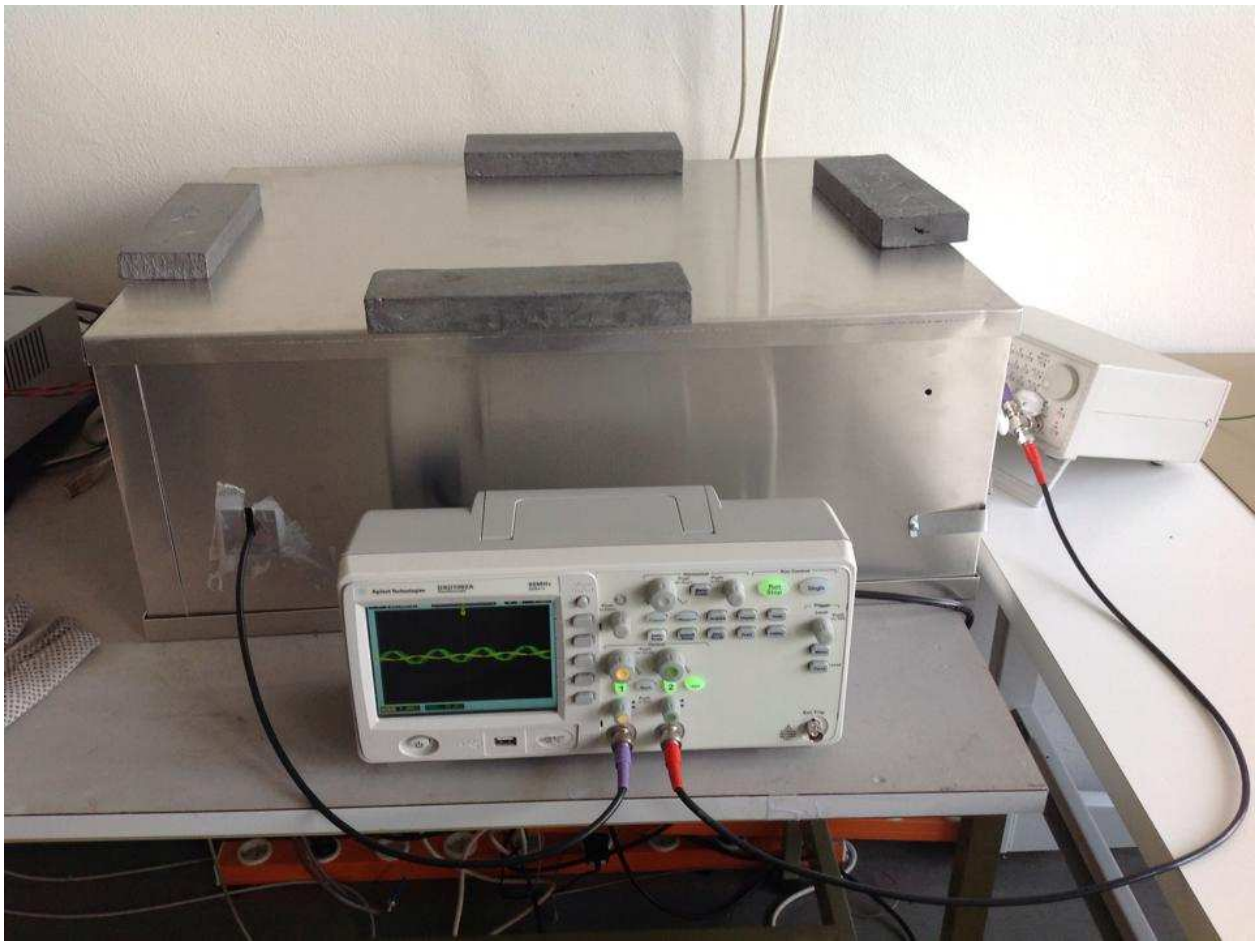

Figure (3.4): The experimental set-up with Oscilloscope in the front, the Faraday cage in the back and the frequency generator to the side of Faraday cage. Oscilloscope shows the waveforms of excitation voltage (measured with the probe with red caps) and pick-up voltage (measured with the probe with pink cap). To make the lid of Faraday cage in perfect contact with the main body, four Fe-blocks are placed on the top.

Chapter 4: Results and Discussion

The experiment we performed were the variation of pick –up voltage with distance, variation of the ratio of pick-up voltage to the excitation voltage with frequency for different distances, effect in the pick-up voltage with insertion of thin steel foil (that is used for baking) and effect of salt solution. The results obtained are discussed with explanation.

4.1 Variation of Efficiency with separation between coils

Since $P = \frac{V^2}{R}$, it is clear that power appearing is proportional to square of voltage, i.e. $P \alpha V^2$. The efficiency will, therefore, be given by

$$P = \frac{P_{pick-up}}{P_{excitation}} = \frac{V^2_{pick-up}}{V^2_{excitation}} = \left(\frac{V_{pick-up}}{V_{excitation}}\right)^2$$

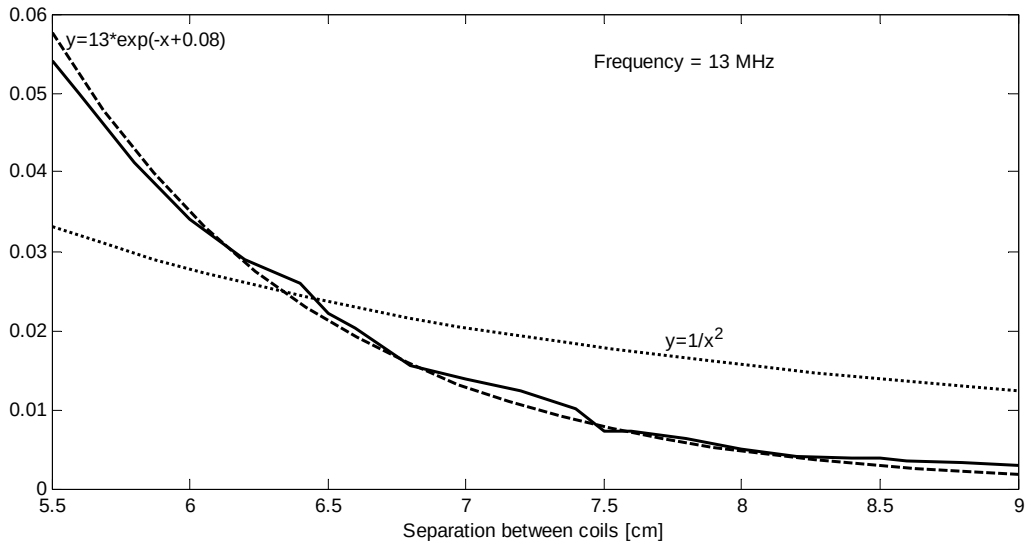

Figure (4.1): *Variation of efficiency (square of the ratio of pick-up voltage and excitation voltage), the solid curve, with distance. The dotted line is an exponential curve fitted to match with experimentally obtained solid curve. The inverse square fitting (small but close dots) does not resemble (it is almost flat) with experimental curve. The curve was plotted at resonant frequency of the coils.*

The exponential fitting is seen to be in close resemblance with experimental whereas the curve corresponding to inverse square law fitting can be seen far deviated from experimental. Instead of just using $\frac{1}{x^2}$, if we use $\frac{A}{x^2}$ and vary the value of A, it can be seen that for lower values of x (here, linspace(5.5,9,20) represents the distance values starting from 5.5cm to end at 9cm with 20 pionts in between), the curve starts form the lower value in y-axis and goes almost below the experimental curve. Whereas, for larger values of A, it starts to shift upwards. On the other hand trying for different values of magnitude term and phase term, the best exponential fit that finds itself in close proximity with exponential curve is chosen to be $y = 13\exp(-x + 0.008)$. The fittings for inverse cubic and inverse 6^{th} power in distances were done (not shown in graph). But these fittings were far deviated from the experimental curve. It can, therefore, be concluded from the plot (4.1) that the efficiency of power transfer shows exponential decrement with increment in separation between coils.

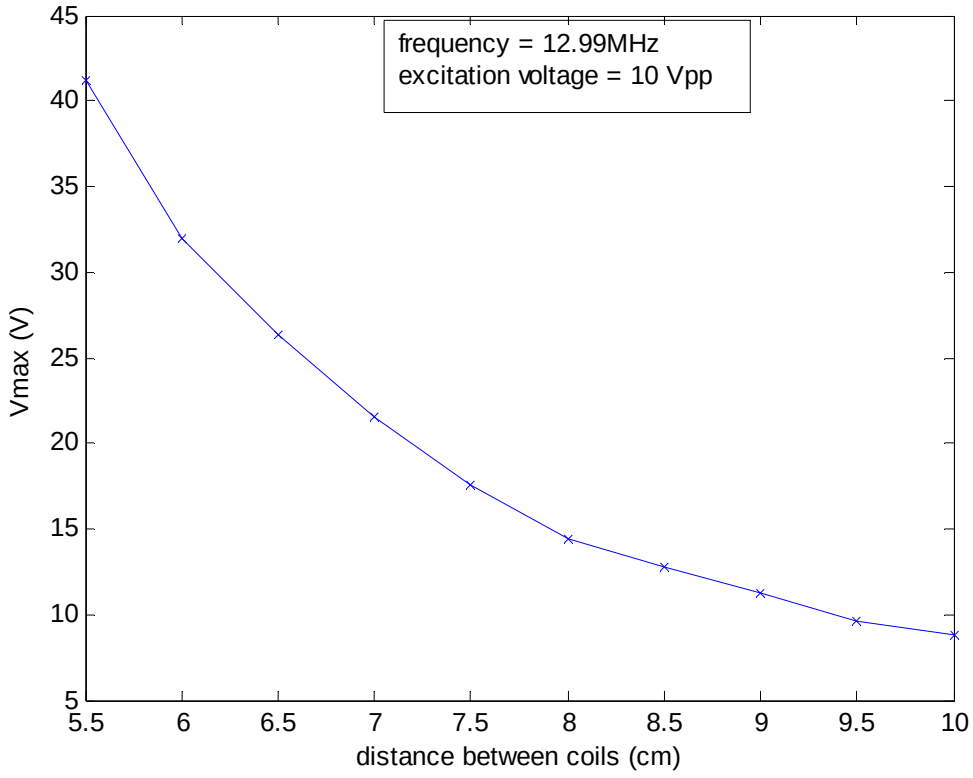

Figure (4.2): *Variation of peak value of pick-up voltage with separation between coils at 12.99MHz, a frequency very close to resonance*

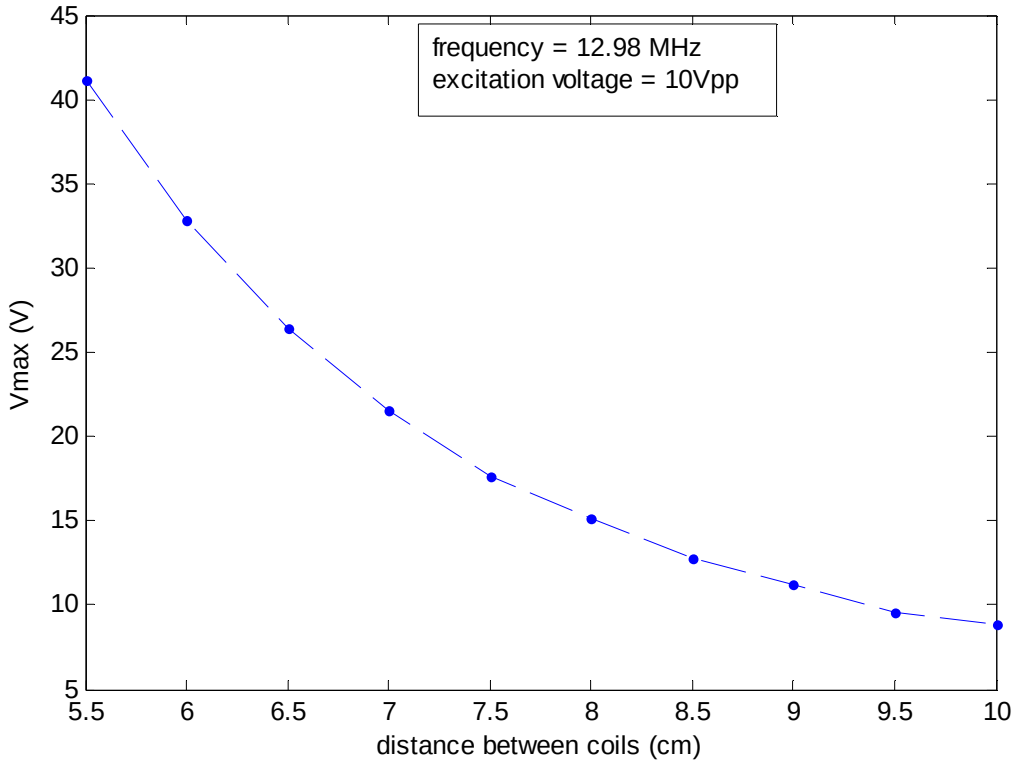

Figure (4.3): *Variation of peak- value of pick up voltage with separation between the coil at 12.98 MHz a frequency close to resonance frequency.*

Figures (4.2) and (4.3) show that with the increase of distance between the coils, the pick-up voltage goes on decreasing almost exponentially as in figure (4.1). This may be due to absorption of power due to air so that less power is available in the pick-up coil. These curves are shown just for the fact that the variation is same as graph (4.1).The unexpectedly large value of pick-up voltage as compared to excitation voltage may be due to noise present and possibly due to the reflection. At the time we did experiment, Faraday cage was not made. So, the presence of noise is justified. The curves shown below for fitting show considerable pick-up voltage values as these measurements were done after making Faraday cage.

4.2 Non- Linear fitting of Resonance Curves

We used non-linear least squares to fit a Lorentzian curve to the data for three different separations of 6cm, 7cm and 8cm between coils. The fitting model is in the Appendix.

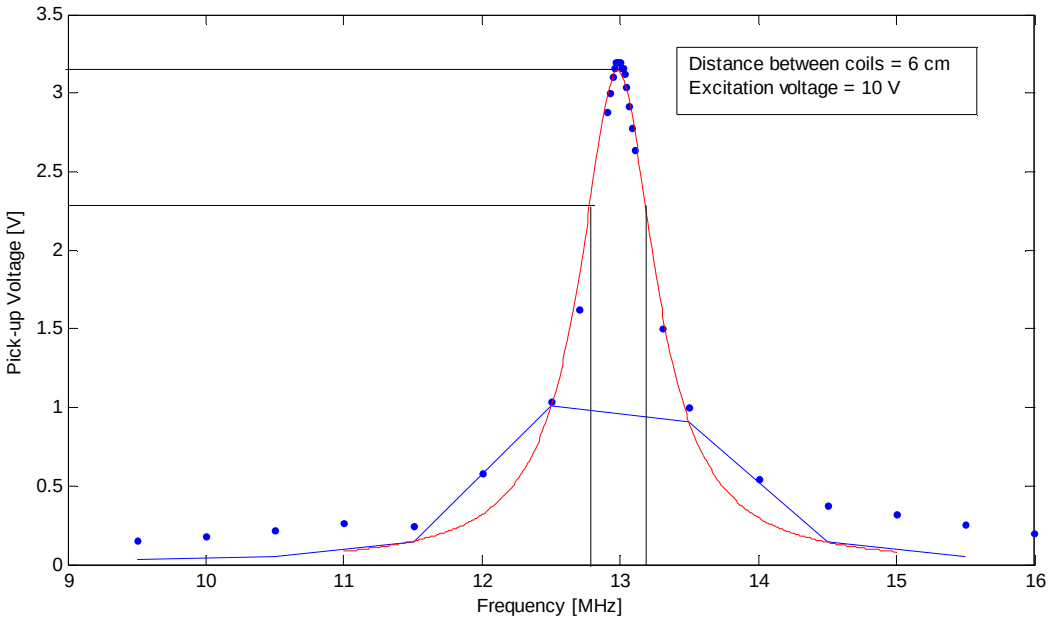

Figure (4.4): *variation of pick-up voltage with frequency at a separation of 6cm between coils. Red curve is the nonlinear fitted curve whereas blue points are the experimentally obtained values.*

From this, we can find the Q-factor knowing the pick-up voltages corresponding to half power i.e. knowing $\frac{1}{\sqrt{2}}$ times the voltage values corresponding to the peak. Then below the frequency axis, we can see two frequency values called half power points. The frequency gap between these two give bandwidth, Δf. Resonance frequency divided by this band width gives the Q-factor. The example is included for the case of figure (4.5).

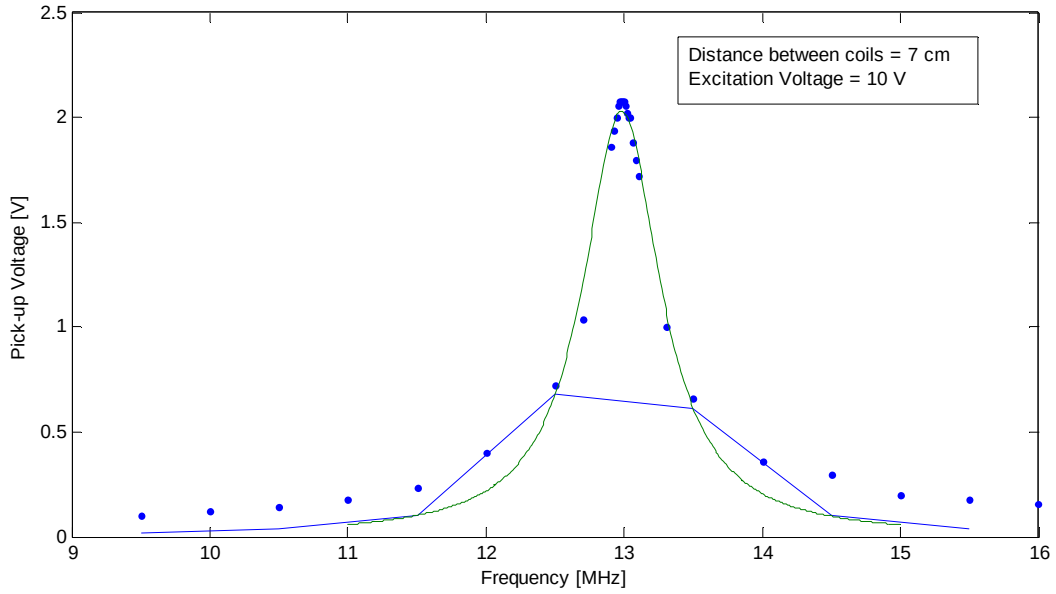

Figure (4.5): *variation of pick-up voltage with frequency at a separation of 7cm between coils*

Half power voltage = 1.44V

Lorentzian fitting of resonance:

Lower half power frequency ≈12.7 MHz

Upper half power frequency ≈13.3 MHz

Q-factor of the system $= \frac{f_r}{\Delta f} \approx \frac{13}{13.3-12.7} = 21.67$

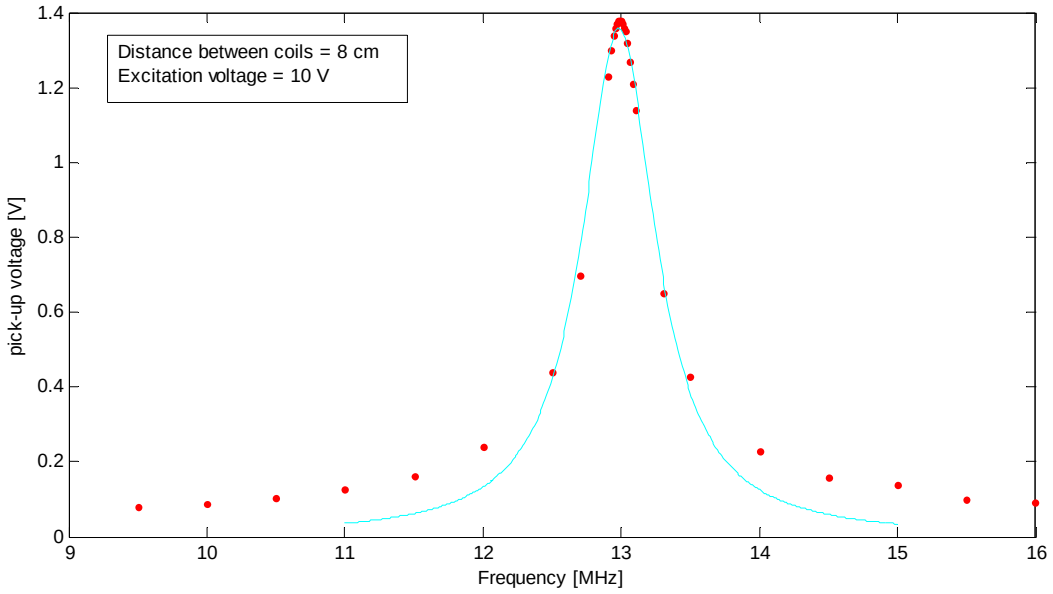

Figure (4.6): *variation of pick-up voltage with frequency at a separation of 8cm between coils*

Comparing figures (4.4), (4.5) and (4.6), is obvious that as the coils come closer to one another, the peak value of pick-up voltage gets greater at resonant frequency and , of course, at other frequencies as well. This will clearly increase the ratio of pick-up voltage to the excitation voltage as there is no significant change in excitation voltage and hence efficiency increases as the coils come closer.

4.3 Effect of Thin Steel foil in power transfer

Placing a thin steel foil in about midway between the coils with the help of a plexi-glass stand, and noting excitation and pick-up, voltages, we recorded 22 files in USB for each frequency selected. The rms values of these csv files can be found using Matlab. In previous cases also we did the same. Following is the resonance curve for this case.

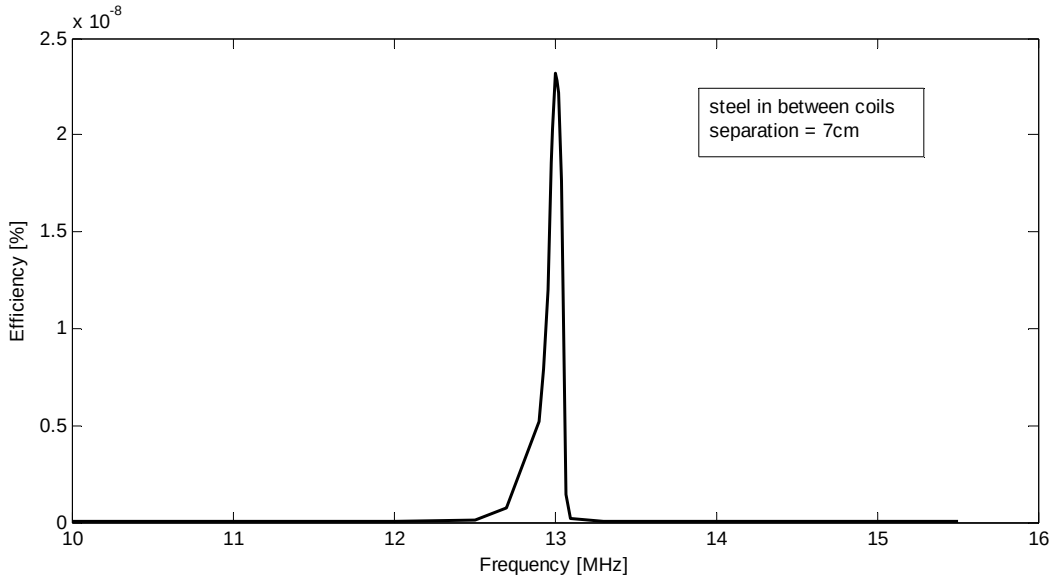

Figure (4.7): *Efficiency of power transmission system in presence of steel in between coils.*

It can be seen that maximum efficiency is hugely reduced without affecting the resonance frequency. So power gets attenuated huge factor when conducting substances like steel foil even of very small thickness is present in the line of sight of the power transmission.

4.4 Effect of Salt-water Solution

10gm of salt was weighed and a solution was made in 250 ml water. After completely dissolving the salt, it was placed in between coils making inter-coil distance of 7.5cm. The curve obtained for this case is less distorted as compared to steel foil in between coils. The attenuation of transferred power is less in this case.

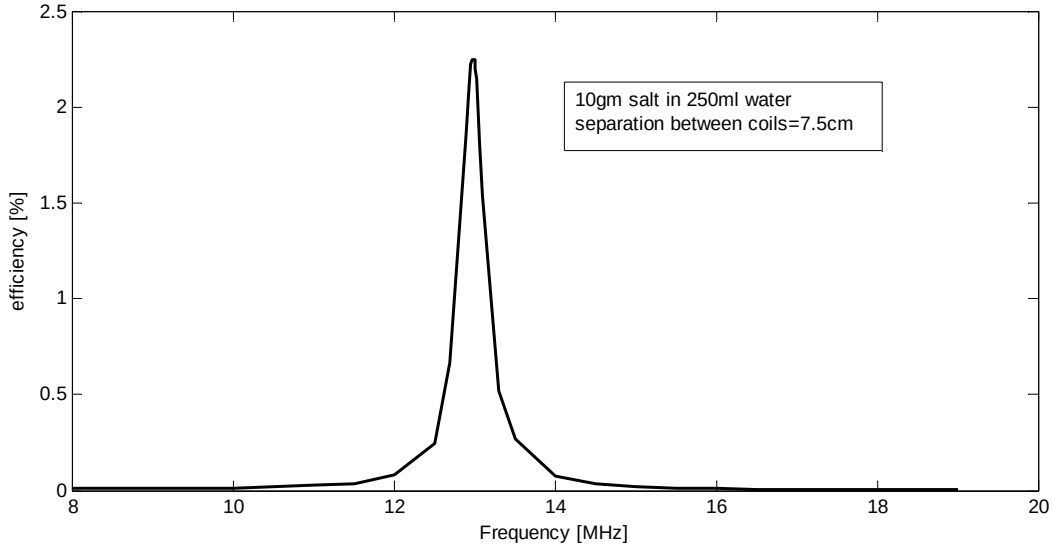

Figure (4.8): *Variation of efficiency with frequency for 10gm salt dissolved in 250ml water, inter-coil separation being 7.5 cm.*

It is seen that the ratio corresponding to each frequency and of course at resonant frequency is reduced as compared to air in between the coils. The reduction in the pick amplitude may correspond to the opposite voltage induced in the solution. The important point to be noticed here is that no shift in resonant frequency is observed on introducing the salt solution in between the coils.

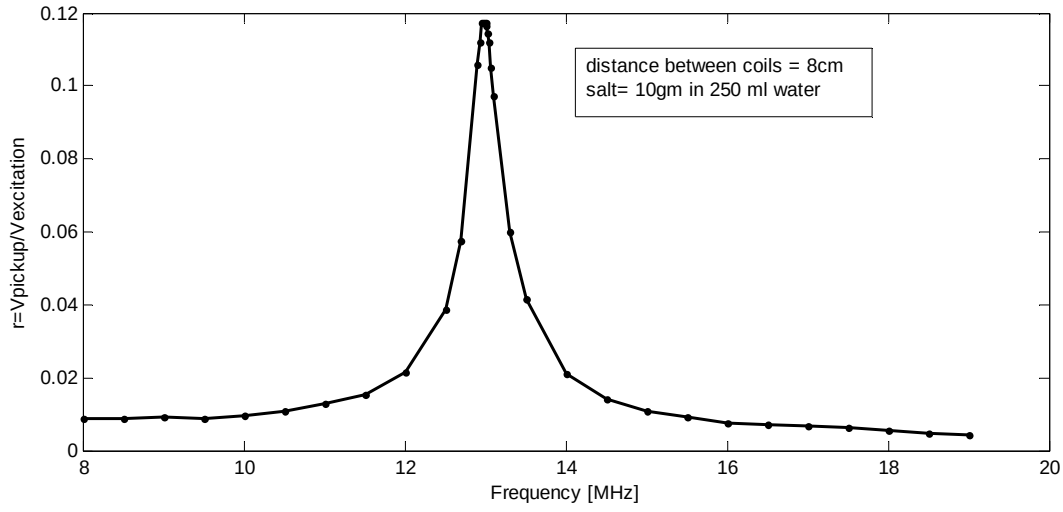

Figure (4.9): *Variation of the ratio of pick up voltage to excitation voltage when distance between coils is 8 cm and the salt solution with 10 gm in 250 ml water is placed in between coils.*

The maximum ratio of around 0.1172 corresponds to the resonance frequency of 13 MHz as compared to around 0.14 with air in between the coils at same resonant frequency. This also indicates that with the salt solution in between the coils the transfer ratio gets decreased.

Chapter 5

Conclusion

In this work, we performed the study of efficiency of wireless power transfer using PCB coils. The power transfer is found to be more when the coils are closer to each other in air. On increasing the distance between coils, the power transfer efficiency is found to decrease exponentially. Here we checked different possibility of inverse square law dependence of power transfer in distance. However, this fitting was not in agreement with experimental curve. So exponential decrement of transmitted power can be assumed with the variation of inter-coil distance.

The variation of power transfer efficiency with frequency for different distances between coils is studied. We found that maximum power is transferred at resonance frequency, which is obvious.

The use of steel foil in the line of sight of power transfer is found to attenuate transferred power to large extent. That means metallic objects degrade power transfer.

Lastly, we used salt solution to check its effect on efficiency of power transfer. Single concentration measurement (using 10gm salt in 250 ml water) shows that even power is attenuated due to its presence on the power transfer path, the degree of attenuation is very small as compared to thin (though) steel foil.

The concluding remark of the project is thus, power transfer is more at resonant frequency when air is present in between coils for closer distances; the power transfer attenuation is more when steel is present in between coils than salt-water solution.

Recommendation

Using perfectly made Faraday cage and taking measurements by handling with LabVIEW would reduce error in the measurement rather than doing the experiment manually.

The method could be used for the conductivity determination of salt solution using different concentration of salt-water concentration and measuring the power transfer efficiency.

Use of meta-material and *Perfect Magnetic Conductors* (PMCs) can be made for increasing power transfer.

References

1) A. Kurs, A. Karalis, R. Moffatt, J. Joannopoulos, P. Fisher, and M. Soljacic, *''Wireless power transfer via strongly coupled magnetic resonances,'' Science, vol. 317, no. 5834, pp. 83–86, Jun. 2007.*
2) http:www.witricity.com
3) http://www.wirelesspowerconsortium.com
4) T Imura, H Okabe, Y Hori, *Basic Experimental Study on Helical Antennas of Wireless Power Transfer for Electric Vehicles by using Magnetic Resonant Couplings*, Vehicle Power and Propulsion …, 2009 - ieeexplore.ieee.org
5) Huang, D., Y. Urzhumov, D. R. Smith, K. H. Teo, and J. Zhang, "Magnetic superlens-enhanced inductive coupling for wireless power transfer," Journal of Applied Physics, Vol. 111, 064902, 2012.
6) Fan et al., *experimental study of efficient wireless power transfer system integrating with highly sub-wavelength metamaterials*, Progress In Electromagnetics Research, *Vol. 141, 769–784, 2013*
7) Jackson J. D., *Classical Electrodynamics*, 3rd Edition, John Wiley and Sons
8) Reitz, Milford and Christy, *Foundations of Electromagnetic Theory, Fourth Edition, Addison-Wesley Publishing Company*
9) Bjarte Lofnes Hauge, *Master's Thesis*, University of Bergen, 2010
10) Takehiro Imura, Member, IEEE, and Yoichi Hori, Fellow, IEEE, IEEE TRANSACTIONS ON INDUSTRIAL, *Maximizing Air Gap and Efficiency of Magnetic Resonant Coupling for Wireless Power Transfer Using Equivalent Circuit and Neumann Formula*, ELECTRONICS, VOL. 58, NO. 10, OCTOBER 2011.
11) Cannon et al., *Magnetic Resonant Coupling As a Potential Means for Wireless Power Transfer to Multiple Small Receivers*, IEEE TRANSACTIONS ON POWER ELECTRONICS, VOL. 24, NO. 7, JULY 2009
12) Wu, J.; Wang, B.; Yerazunis, W.S.; Teo, K. H., *Wireless Power Transfer with Artificial Magnetic Conductors*, Mitsubishi Electric Research Laboratories, http://www.merl.com.
13) TeckChuan Beh, Masaki Kato, Takehiro Imura, Yoichi Hori, *Wireless Power Transfer System via Magnetic Resonant Coupling at Fixed Resonance Frequency - Power Transfer System Based on Impedance Matching*, World Electric Vehicle Journal Vol. 4 - ISSN 2032-6653 - © 2010 WEVA.

14) Kim et al., *Coil Design and Shielding Methods for a Magnetic Resonant Wireless Power Transfer System*, Proceedings of the IEEE | Vol. 101, No. 6, June 2013

15) Introduction to Electrodynamics, 3rd edn, David J. Griffiths, Prentice Hall

16) Hermann A. Haus, *Chapter 7, Waves and Fields in Optoelectronics*, Prentice-Hall series in Solid State Physical Electronics

17) *ieeexplore.ieee.org/iel5/5510786/5521890/05521939.pdf?arnumber*

18) Lipworth G. et.al, *Magnetic Metamaterial Superlens for Increased Range Wireless Power Transfer*, Scientific Reports,4 Article number 3642, 2014.

19) A. S. Y. Poon, S. O'Driscoll, and T. H. Meng, *IEEE Trans. Antennas Propag. 58, 1739–1750 (2010).*

20) http://www.qinside.biz/en/faq/what-is-wireless-charging

21) N. Tesla, U.S. patent 1,119,732(1914)

22)*ocw.mit.edu/courses/electrical...and.../6.../**resonance**_qfactr.pdf*

23)http://www.ti.com/

24)Avraham klein and Nadav Katz, *Strong Coupling Optimization with Planar Spiral Resonators*, Current Applied Physics 11(2011) 1188-1191

Appendix

For the non-linear fitting of our experimental data , we used the non-linear least squares to fit a Lorentzian curve provided by Lars Egil Helseth and in Master's thesis of Bjarte Lofnes Hauge [9]:

```
%We use nonlinear least squares to fit a Lorentzian curve to the data
For example,
x=[10 10.5 11 11.5 12 12.5 12.9 12.93 12.96 12.98 12.99 13 13.01 13.02 13.04 13.07 13.1
13.5 14 14.5 15 15.5 16];

y=[0.08 0.096 0.139 0.178 0.256 0.385 0.500 0.656 0.800 0.959 1.120 1.44 1.83 2.20 1.9 1.55
1.28 1.02 0.88 0.72 0.66 0.52 0.426];



f_min=10;
f_max=16;
f_fit=f_min:f_max;
Y_fit=@(p,x) p(1)./((x-p(2)).^(2) + p(3));

w3=10; %guess a parameter p3
w2=12; %guess a parameter p2 (resonance frequency)
w1=12; %guess a parameter p1
w0=[w1,w2,w3];


best = nlinfit(x, y, Y_fit, w0');
line(f_fit, Y_fit(best(:,1), f_fit));
hold on


C2=best(2);              %Find the resonance frequency
C1=best(1);                    %Find the fitted w1
C3=best(3);                    %Find the fitted w2
```

```
w=10:0.1:16;
Y_theory=C1./((w-C2).^(2) + C3);

plot(x,y,'square',w,Y_theory)
```